AD-785 377

SEISMIC DISCRIMINATION

Michael A. Chinnery

Massachusetts Institute of Technology

Prepared for:

Electronic Systems Division
Advanced Research Projects Agency

30 June 1974

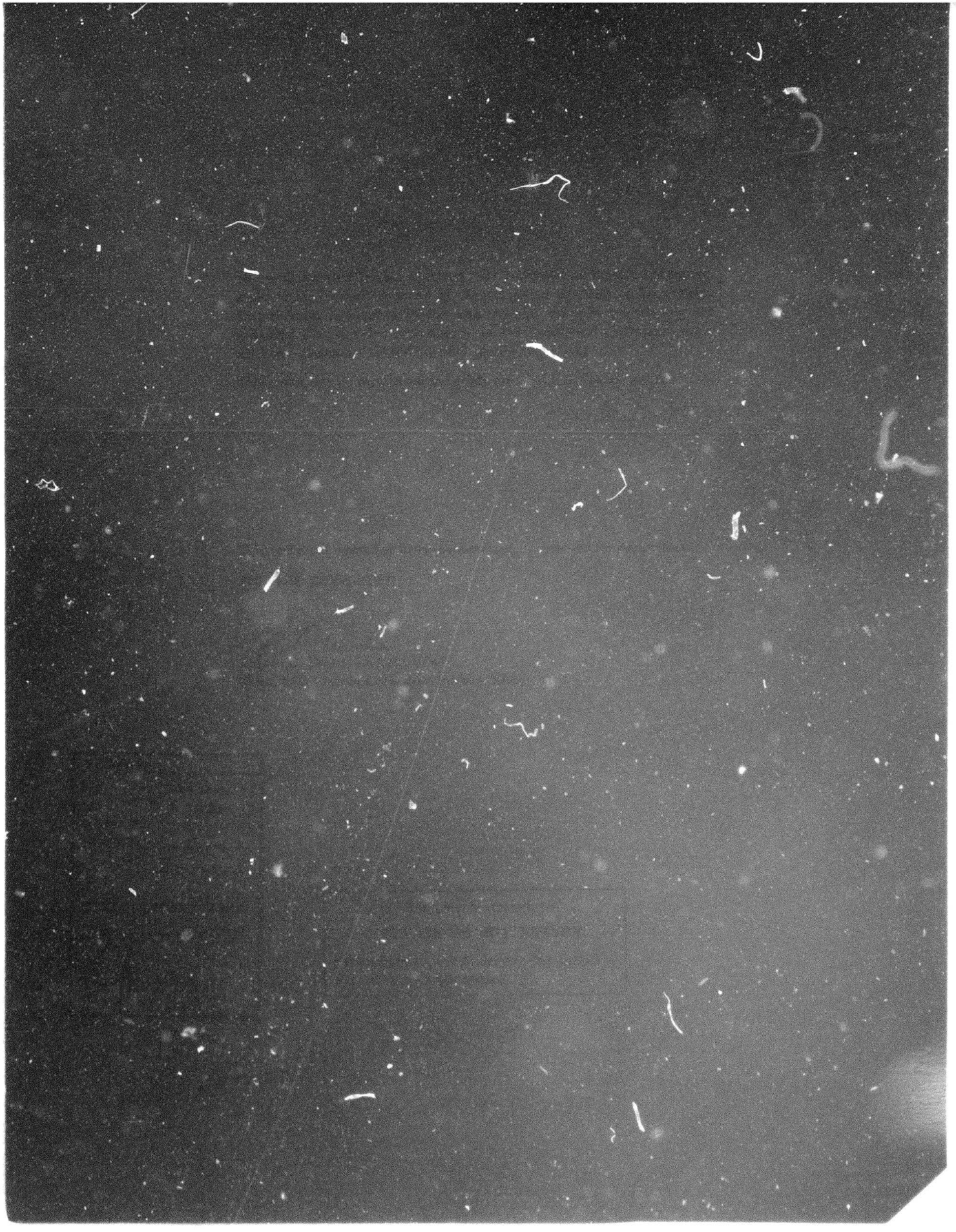

UNCLASSIFIED

SECURITY CLASSIFICATION OF THIS PAGE *(When Data Entered)*

AD-785377

REPORT DOCUMENTATION PAGE		READ INSTRUCTIONS BEFORE COMPLETING FORM
1. REPORT NUMBER ESD-TR-74-221	2. GOVT ACCESSION NO.	3. RECIPIENT'S CATALOG NUMBER
4. TITLE *(and Subtitle)* Seismic Discrimination		5. TYPE OF REPORT & PERIOD COVERED Semiannual Technical Summary, 1 January – 30 June 1974 6. PERFORMING ORG. REPORT NUMBER
7. AUTHOR(s) Chinnery, Michael A.		8. CONTRACT OR GRANT NUMBER(s) F19628-73-C-0002
9. PERFORMING ORGANIZATION NAME AND ADDRESS Lincoln Laboratory, M.I.T. P.O. Box 73 Lexington, MA 02173		10. PROGRAM ELEMENT, PROJECT, TASK AREA & WORK UNIT NUMBERS ARPA Order 512
11. CONTROLLING OFFICE NAME AND ADDRESS Advanced Research Projects Agency 1400 Wilson Boulevard Arlington, VA 22209		12. REPORT DATE 30 June 1974 13. NUMBER OF PAGES 72
14. MONITORING AGENCY NAME & ADDRESS *(if different from Controlling Office)* Electronic Systems Division Hanscom Air Force Base Bedford, MA 01730		15. SECURITY CLASS. *(of this report)* Unclassified 15a. DECLASSIFICATION DOWNGRADING SCHEDULE

16. DISTRIBUTION STATEMENT *(of this Report)*

Approved for public release; distribution unlimited.

17. DISTRIBUTION STATEMENT *(of the abstract entered in Block 20, if different from Report)*

18. SUPPLEMENTARY NOTES

None

19. KEY WORDS *(Continue on reverse side if necessary and identify by block number)*

seismic discrimination
seismic array
seismology
surface waves
LASA
body waves
NORSAR
ARPANET

20. ABSTRACT *(Continue on reverse side if necessary and identify by block number)*

The basic compilation and analysis of the seismic data during the International Seismic Month have been completed. We have become involved in the development of management systems for global seismic data and network documentation. We are beginning to focus our attention on earthquake source mechanisms and the determination of focal depth; some initial results are described. We continue to evaluate the effects of earth heterogeneity both on surface waves and body waves. Development of a seismic computer terminal system for the ARPA network is progressing satisfactorily.

DD FORM 1 JAN 73 1473 EDITION OF 1 NOV 65 IS OBSOLETE

UNCLASSIFIED

SECURITY CLASSIFICATION OF THIS PAGE *(When Data Entered)*

MASSACHUSETTS INSTITUTE OF TECHNOLOGY

LINCOLN LABORATORY

SEISMIC DISCRIMINATION

SEMIANNUAL TECHNICAL SUMMARY REPORT
TO THE
ADVANCED RESEARCH PROJECTS AGENCY

1 JANUARY - 30 JUNE 1974

ISSUED 5 AUGUST 1974

LEXINGTON MASSACHUSETTS

ABSTRACT

The basic compilation and analysis of the seismic data during the International Seismic Month have been completed. We have become involved in the development of management systems for global seismic data and network documentation. We are beginning to focus our attention on earthquake source mechanisms and the determination of focal depth; some initial results are described. We continue to evaluate the effects of earth heterogeneity both on surface waves and body waves. Development of a seismic computer terminal system for the ARPA network is progressing satisfactorily.

CONTENTS

SUMMARY

This is the twenty-first Semiannual Technical Summary report describing the activities of Lincoln Laboratory, M.I.T., in the field of seismic discrimination. These activities involve research into the fundamental seismological problems associated with the detection, location, and identification of earthquakes and nuclear explosions. We are also concerned with the development of methods for the handling and analysis of large quantities of global seismic data, both from the point of view of data management system design, and also to facilitate the optimum extraction of scientific information from high-quality digital data.

A major achievement during the current research period has been the completion of the basic compilation of seismic data for the International Seismic Month (ISM). These results have been published in the form of two Lincoln Laboratory Technical Notes (1974-14 and 1974-15), and the highlights of these final reports are described in this SATS. The event list will form an ideal data base for a variety of studies in seismic discrimination, and the experience gained during the study is expected to have a significant impact on any future operational monitoring scheme.

We are becoming heavily involved in the design of the data management system that will accompany the new seismic instrumentation currently being deployed by DARPA NMRO. Our basic charge is to ensure that the acquisition, flow, and storage of these new digital data meet the requirements of those groups actively engaged in studies related to seismic discrimination. A related aspect of this work involves the exploitation of the full power of the computational facilities of the ARPANET for the storage, transmittal, and retrieval of both seismic data and the associated network documentation. Development of these systems is still in an early stage, and a brief progress report is included in this SATS.

With the completion of the bulk of the data analysis associated with the ISM, we are embarking on a series of investigations into the mechanism and focal depth of the seismic source. Some initial results are outlined in this SATS. It is shown that average M_s-m_b and moment-M_s relationships place bounds on acceptable theories for the spectral characteristics of the seismic source. Information about these relationships can be deduced from frequency-magnitude curves. Other studies are concerned with the effects of upper-mantle structure on focal mechanism solutions, and the determination of source dimensions for earthquakes in a localized geographical region.

Investigations into the determination of the focal depth of seismic events are proceeding in several directions, two of which are described here. It is demonstrated that maximum entropy spectral analysis may be applied to the identification of depth phases by the location of cepstral peaks. This method appears promising. Another study continues our analysis of the estimation of focal depth from surface wave spectra. It is shown that certain earth structures that are consistent with observed surface wave dispersion curves can lead to very inaccurate depth estimates. It is not yet clear that this method has any useful application to the seismic discrimination problem, particularly at low magnitudes.

Our studies of the effects of earth structure and path variations have continued, and have been concerned with both surface and body waves. We have achieved further success in predicting the refraction and multipathing of Rayleigh waves by lateral variations in crustal structure. Using body waves, we have completed a refined version of the amplitude-distance curve, and discuss the nature of precursors to pP, S, and SKS from certain deep focus events. Two other

studies describe body wave scattering, one as upper-mantle structure affects PcP/P amplitude ratios, and the other as crustal inhomogeneities affect the P-wave coda at short distances.

Finally, we outline three investigations that are continuations of earlier work. Our study of the tectonics of Asia includes a detailed analysis of the Baikal Rift Zone; we conclude our analysis of NORSAR travel time anomalies by discussing their extension into aseismic regions, and we show an application of the single-channel event detector described in the preceding SATS.

We are developing a sophisticated interactive computer facility as an in-house research capability that will enable us to access and manipulate seismic data once they become available on the ARPANET. Progress in the design of the appropriate software is continuing, and will be reported in more detail in the next SATS.

M. A. Chinnery

GLOSSARY

ARPANET	ARPA Computer Network
DADS	Data Analysis and Display System
DARPA (ARPA)	Advanced Research Projects Agency
GMT	Greenwich Mean Time
ISC	International Seismological Center
ISM	International Seismic Month
IWWSS	Integrated World-Wide Seismic System
LASA	Large Aperture Seismic Array
LTA	Long-Term Average
NLS	On-Line System
NMRO	Nuclear Monitoring Research Office
NOAA	National Oceanic and Atmospheric Administration
NORSAR	Norwegian Seismic Array
PDE	Preliminary Determination of Epicenters
SATS	Semiannual Technical Summary
STA	Short-Term Average
TENEX	PDP-10 Operating System
USCGS	United States Coast and Geodetic Survey
USGS	United States Geological Survey
VESPA	Velocity Spectral Analysis

SEISMIC DISCRIMINATION

1. INTERNATIONAL SEISMIC MONTH

A. INTERNATIONAL SEISMIC MONTH (ISM) FINAL EVENT LIST

Final adjustments have been made to the ISM[1,2] Event List. The resulting list of 996 events and some discussion of its statistics have been published in a recent Technical Note.[3]

The ISM detection and location threshold has been estimated world-wide and for Asia. For this purpose, Asia was defined using standard seismic regions.[4] Specifically, we took Asia to be composed of the seismic regions listed in Table 1-1. Figure 1-1 shows a cumulative histogram of the m_b values for the 859 ISM events for which we were able to determine magnitudes and for the subset of events in Asia. In the Asian region there were 215 events with m_b assigned, and 33 with no m_b determined.

TABLE I-1
SEISMIC REGIONS DEFINING ASIA FOR THE ISM

Region No.	Region Name
19	Japan-Kuriles-Kamchatka
26	India-Tibet-Szechwan-Yunan
27	Southern Sinkiang to Kansu
28	Alma-Ata to Lake Baikal
29	Western Asia
30	Middle East-Crimea-Balkans
41	Eastern Asia
42	N. E. Asia, Northern Alaska to Greenland
47	Baluchistan
48	Hindu Kush and Pamir
49	Northern Asia

It is often assumed that the log of the number of events for a fixed time interval in any region will vary linearly with m_b. One can then fit straight lines to histograms such as those on Fig. I-1 and estimate at what magnitude level the detection system seems to start missing events. Basham and Anglin[5] used preliminary ISM data for a region similar to our Asian region and concluded that the cumulative 90-percent detection threshold for that region was about 4.0. Since incremental thresholds are normally 0.2 to 0.3 units higher,[6] they estimated the 90-percent incremental threshold to be 4.3 for that region. The data of Fig. 1-3 do not contradict the conclusion, although this fitting of straight lines must be accepted with some skepticism as a method of estimating detection thresholds since it does use a theoretically unsubstantiated assumption about the linear variation of seismic activity with m_b.

Fitting the complete ISM cumulative occurrence of events to obtain a detection and location threshold is doubly bothersome. Not only must the straight-line assumption be accepted, but it is even more difficult to find a straight region to fit with a straight line. However, if such a

method is used, it is our estimate that the 90-percent cumulative threshold obtained is between 4.5 and 4.6, with the corresponding incremental threshold 0.2 to 0.3 m_b units higher.

These detection capabilities have been further substantiated by comparisons with LASA and NORSAR bulletins. Details will be found in Lacoss, et al.[3]

Only recently has the Bulletin of the International Seismological Center (ISC) been published for the ISM time period. Since this is the most comprehensive regular bulletin prepared at this time, it is of interest to compare it with the ISM list.

TABLE I-2

DISTRIBUTION BY GRADE AND m_b OF THE 481 ISM EVENTS WHICH DID NOT APPEAR ON THE ISC BULLETIN

Grade	No. of Events	m_b	No. of Events
A	49	0.0	84
AI	35	<3.5	44
B	17	3.5-3.59	25
BI	9	3.6-3.69	30
C	27	3.7-3.79	27
CI	22	3.8-3.89	34
D	137	3.9-3.99	35
DI	185	4.0-4.09	39
		4.1-4.19	32
		4.2-4.29	32
		4.3-4.39	28
		4.4-4.49	26
		>4.5	45

The ISC reported 515 of the 996 ISM events (51.8 percent). The distribution of grade[1,3] and m_b for the ISM events not reported by the ISC is given in Table I-2. Conversely, the ISC Bulletin reported 299 events during this period that did not appear on the ISM list. Of these 299 events, 76 had 3 or less reporting stations, 72 had their farthest reporting station within 3° of the epicenter, and 113 events did not have more than 3 of the stations used in the ISM study among their reporting stations. A breakdown of the remaining 38 events, of which 3 events (denoted by *) were reported on the ISM unverified array event list,[3] that possibly could have met ISM acceptance criteria is shown in Table I-3. The magnitudes listed in this table are of various kinds as reported by the ISC with only the teleseismic body wave magnitude m_b being directly comparable to the ISM magnitude. The others are: ML, local magnitude; M, magnitude (unspecified); and M_s, surface-wave magnitude. In general, it would appear that no events above the claimed ISM detection thresholds appeared on the ISC Bulletin.

There are two primary reasons why these 38 ISC events did not appear in the ISM event list. In some cases, arrivals were associated but we rejected the resulting hypocenter because of poor residuals or insufficient control on the hypocenter. More commonly, we failed to ever associate the arrivals with a single event.

TABLE I-3

ISC BULLETIN EVENTS NOT CONTAINED IN THE ISM LIST. ALL MISSED ISC EVENTS WITH 3 OR MORE ISM STATIONS REPORTING AND AT LEAST ONE STATION MORE THAN 3° FROM THE EPICENTER ARE INCLUDED.

Location	No. of ISC Reporting Stations	No. of ISM Stations	Greatest Δ of ISC Stations (deg)	Magnitude
Austria	13	7	3.96	1.6 ML
New Hebrides	4	4	4.80	3.8 m_b
New Hebrides	6	4	5.62	3.4 m_b
Off Coast No. California	8	4	9.32	3.8 ML
New Hebrides	5	4	4.10	3.7 m_b
New Hebrides	5	4	6.84	4.0 m_b
New Hebrides	4	4	4.63	3.4 m_b
New Hebrides	5	4	7.60	4.0 m_b
So. Africa	6	4	10.05	3.3 M
New Hebrides	9	8	151.51	3.9 m_b
Norwegian Sea	7	5	10.97	–
So. Africa	6	5	9.41	3.5 M
So. Africa	8	5	11.00	4.0 m_b
E. Caucasus	13	5	65.56	3.6 M_s
New Hebrides	6	5	32.95	3.4 m_b
Hindu Kush	6	5	74.72	3.7 m_b
No. California	7	4	5.54	3.5 ML
* Greece	11	3	25.61	3.1 ML
No. California	9	6	21.27	3.8 ML
Hindu Kush	5	4	42.96	4.2 m_b
Off Coast No. California	9	6	12.59	4.1 ML
Davis Strait	5	4	35.03	–
Western Caucasus	10	4	26.57	3.7 M_s
No. California	11	6	10.39	3.5 ML
* Hindu Kush	7	6	44.52	3.7 m_b
New Hebrides	8	7	148.05	4.0 m_b
Off E. Coast New Zealand	15	6	151.17	4.4 M
No. Island New Zealand	22	7	146.36	5.0 M
Loyalty Isles Reg.	11	8	98.66	4.7 m_b
* Chile-Argentina Border Reg.	7	6	83.88	–
Off Coast No. California	8	4	7.81	4.1 ML
California-Mexico Border Reg.	9	5	19.34	4.5 ML
Off Coast No. California	7	4	9.90	3.9 ML
So. Africa	15	11	146.11	4.1 M
Loyalty Isles Reg.	5	4	67.38	3.8 m_b
Loyalty Isles Reg.	5	4	33.37	3.8 m_b
New Britain Reg.	10	9	25.06	4.9 ML
Tadzhik	5	4	42.96	–

As explained earlier,[7] the location programs used for the ISM find the origin time and hypocenter which minimize a weighted sum of the squares of observation residuals. An error ellipsoid is defined which corresponds to a unit increase of this sum of squares. From this ellipsoid, we obtain two measures of epicenter quality. One, MAXAX2 is the major semiaxis of the epicenter error ellipsoid. The other, DEPTHQ, is half the vertical extent of the hypocenter error ellipsoid.

Experiments have been completed to calibrate these quality variables. In one of these experiments, all well-recorded events which used depth phases in obtaining a hypocenter were relocated without using the depth phases. Of these, 141 converged properly without any need for restraining depth for the relocation. Since the previous locations with depth phases tended to pin the depth closely to that indicated by the depth phases, we took the difference between the two depths as the actual error in depth for the relocated events. The absolute value of this error was weighted inversely by the depth quality of the relocated event, and the histogram of Fig. I-2 was generated. Accepting the assumption that the original depth was correct, we see that the indicated depth of the relocated events is almost never in error by more than 2*DEPTHQ kilometers and that it is less than DEPTHQ for 75 percent of the relocated events. Other calibration experiments, involving MAXAX2 as well as DEPTHQ, are described in Ref. 3. The results are all similar to those indicated on Fig. I-2.

R. T. Lacoss
R. E. Needham

B. PERFORMANCE OF SELECTED SHORT-PERIOD SITES DURING THE ISM PERIOD

With the completion of the ISM experiment,[3] there is now available a large quantity of station data, both short- and long-period arrival times, amplitudes, etc. A great deal of effort has gone into merging the short-period data for over 30 selected sites with the epicenter location data from the ISM list. The total quantity of data exceeds 350,000 items, all contained on one magnetic tape in a format acceptable to the DADS.[8] With the data in this format, it is now possible to display all or part of it with the DADS. In addition, the complete library of routines, both numerical and graphic, are available to aid in the analysis of single station or sets of stations or in epicenter location or any other related phenomenon.

The analysis of some of the station performance characteristics, which is just beginning, will cover all the stations that reported a substantial number of arrivals during the ISM period, with an emphasis on the Canadian stations. Initially, only the better events, i.e., those reported with a quality of A or AI, will be used in the study. This will give a more reliable base of events that have a large number of stations used for locations and magnitude determinations. For these 375 events with A or AI rating, the station detection levels are shown in Fig. I-3 where it can be seen that only 7 stations detected more than half of the 375 events. Of these 7 stations, 4 are actually seismic arrays whose detection levels were greatly enhanced by beamforming. The remaining 3 stations (MBC, UBO, and KBL) are simply good quality single site seismometers.

The Canadian seismic network data that contributed to the ISM provided a very good quality set of data from a single area. This will provide a good data set to examine variables such as travel time anomalies, magnitude correction terms, and other related factors. One term, the magnitude correction term in the formula for short-period magnitude, has been studied initially. While there are many ways to determine what the magnitude correction values are, the method used here was to plot magnitude of all A and AI events for a given station on a distance/magnitude

plot. Then the outline of the Gutenberg-Richter magnitude "B" factor curve for depth 0 and 700 was overlayed onto the data and fitted to the data by eye. The resulting value on the 0 depth curve at 55° was chosen as the magnitude detection level for that station. The results for the Canadian network are displayed on Fig. I-4 along with possible contours of the magnitude detection levels throughout all of Canada based on the network values. Only one site, SES, shows a radical departure from the pattern. It has an unusually low magnitude detection level. There can be several reasons for this but it is probably due to the very low detection level to the Gulf of California swarm in the ISM.

Continued examination of all factors relating to the ISM list and the station set hopefully will reveal more interesting features in the data and possible explanations of these effects.

R. M. Sheppard
R. E. Needham

C. LONG-PERIOD RESULTS FROM THE INTERNATIONAL SEISMIC MONTH

The first study of the long-period aspects of the ISM has been completed and reported elsewhere[9]; here, we shall only review some of the problems encountered and the results of the study. The chief problems were found in the automatic association of the long-period detections with the epicenter list and in the surface wave magnitude assignments. Only half of the detections were assigned an association by the individual readers, persons with widely varying experience in the interpretation of long-period seismograms. Therefore, to treat all the data in a consistent manner, it was decided to consider all the long-period detections as unassociated and develop various automatic association schemes. The definition of what is an optimum scheme is somewhat arbitrary; a scheme that makes no misassociation will probably give too few true associations to be practical, while another that associates all the readings may make an unacceptable number of mistakes. Various combinations of path dependent group velocity curves and association window lengths were tested; however, it was found that a world average group velocity curve with a ±0.5-km/sec association window gave more unique associations than any other scheme. This latter scheme also gave the best results when compared with the cases where an association was made by the readers. In all, about 55 percent of all the detections identified as main Rayleigh phases were given unique associations by the accepted scheme.

The "Prague" formula for surface wave magnitude determination was used initially, but it was found to give consistent results only near periods of 20 sec, where it was defined. The method described by Marshall and Basham,[10] which uses a path dependent period connection, was then applied and gave much better results, i.e., it yielded consistent magnitudes for an event over a wide range of periods and distances. In order to incorporate the maximum number of long-period detections into the magnitude determinations, the distance tables of Marshall and Basham[10] were extended to 180° and the period corrections were extended from 40 to 100 sec. By using these extended tables, individual M_s values were computed for each associated long-period detection, and an event average M_s and standard deviation were computed.

Figure I-5 shows the distribution of these average M_s values plotted as a function of the m_b of the grade A events. This grade was used to indicate the more accurately located events of the ISM short-period list. The curve represents the distribution of world-wide M_s-m_b data summarized by Aki,[11] and the straight line, due to Gutenberg and Richter,[12] is often used as an M_s-m_b relationship. It is evident that this line is <u>not</u> representative of either Aki's summary curve or

the world-wide ISM data. Figure I-6 gives some indication of capability of the long-period network used in the ISM to detect surface waves from shallow events in Asia. It shows the total number of events of a given m_b or greater, and the number of that total for which a surface wave magnitude based on two or more measurements was computed. Based on this figure, the 90-percent cumulative threshold for M_s, based on two or more measurements, for shallow Asian events during the ISM was about $m_b = 4.6$.

J. R. Filson

REFERENCES

1. Seismic Discrimination SATS, Lincoln Laboratory, M.I.T. (31 December 1973), Sec. I, DDC AD-777151.
2. D. Davies and R. T. Lacoss, "First Results from the International Seismic Month," Technical Note 1973-32, Lincoln Laboratory, M.I.T. (2 July 1973), DDC AD-762921.
3. R. T. Lacoss, R. E. Needham and B. R. Julian, "International Seismic Month Event List," Technical Note 1974-14, Lincoln Laboratory, M.I.T. (27 February 1974), DDC AD-776021/8.
4. E. A. Flinn and E. R. Engdahl, "A Proposed Basis for Geographical and Seismic Regionalization," Rev. Geophys. 3, 123 (1965).
5. P. W. Basham and F. M. Anglin, "Multiple Discriminant Screening Procedure for Test Ban Verification," Nature 246, 474 (1973).
6. R. T. Lacoss, "Seismic Event Detection and Discrimination – Some Statistical Considerations," in Proceedings from the Seminar on Seismology and Seismic Arrays, Oslo, 22-25 November; available from NTNF/NORSAR Kjeller, Norway.
7. Seismic Discrimination SATS, Lincoln Laboratory, M.I.T (30 June 1973), DDC AD-766559/9.
8. Ibid. (31 December 1972), DDC AD-757560.
9. J. R. Filson, "Long Period Results from the International Seismic Month," Technical Note 1974-15, Lincoln Laboratory, M.I.T. (4 March 1974), DDC AD-776089/5.
10. P. Marshall and P. Basham, "Discrimination Between Earthquakes and Underground Nuclear Explosions Employing an Improved M_S Scale," Geophys. J. R. Astr. Soc. 28, 431 (1972).
11. K. Aki, "Scaling Law of Earthquake Source Time Function," Geophys. J. R. Astr. Soc. 31, 3 (1972).
12. B. Gutenberg and C. Richter, "Magnitude and Energy of Earthquakes," Ann. Geofis. 9, 1 (1956).

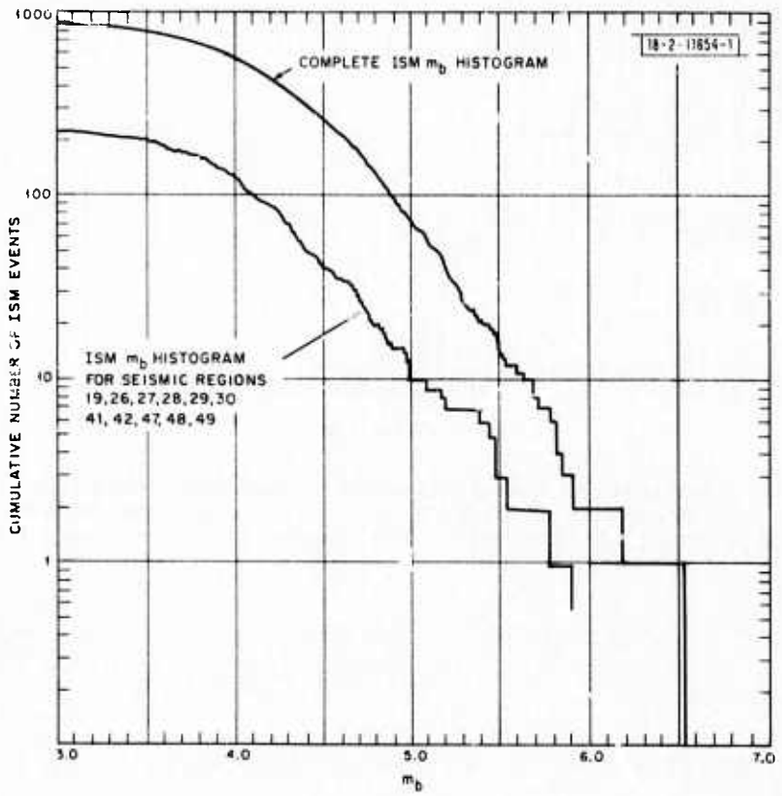

Fig. I-1. Cumulative histogram of complete ISM m_b and for events limited to Asian seismic regions 19, 26, 27, 28, 29, 30, 41, 42, 47, 48, 49.

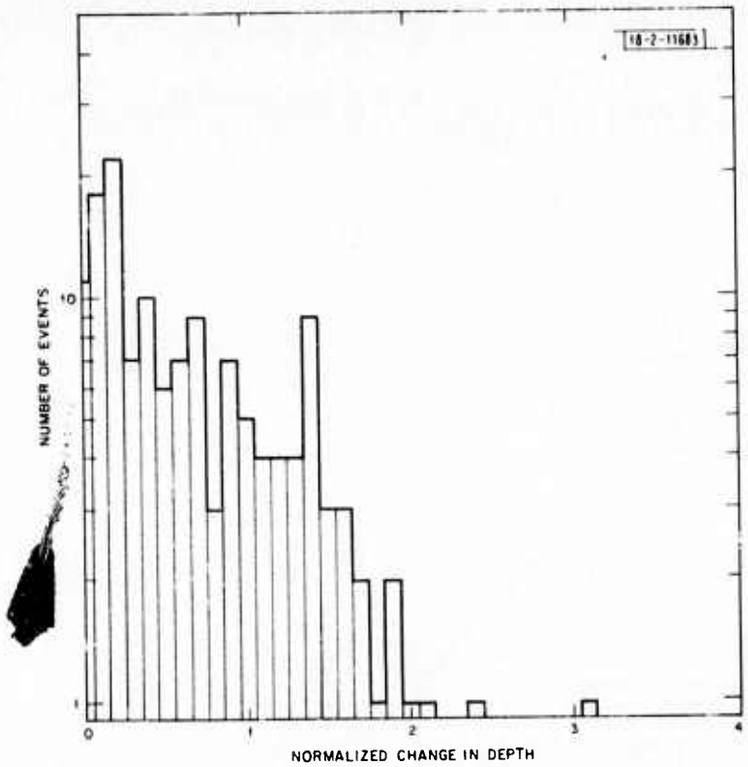

Fig. 1-2. Histogram of change in depth resulting from relocating A grade events after discarding all depth phases. Each change is normalized by relocation depth quality parameter. Total number of events used is 141.

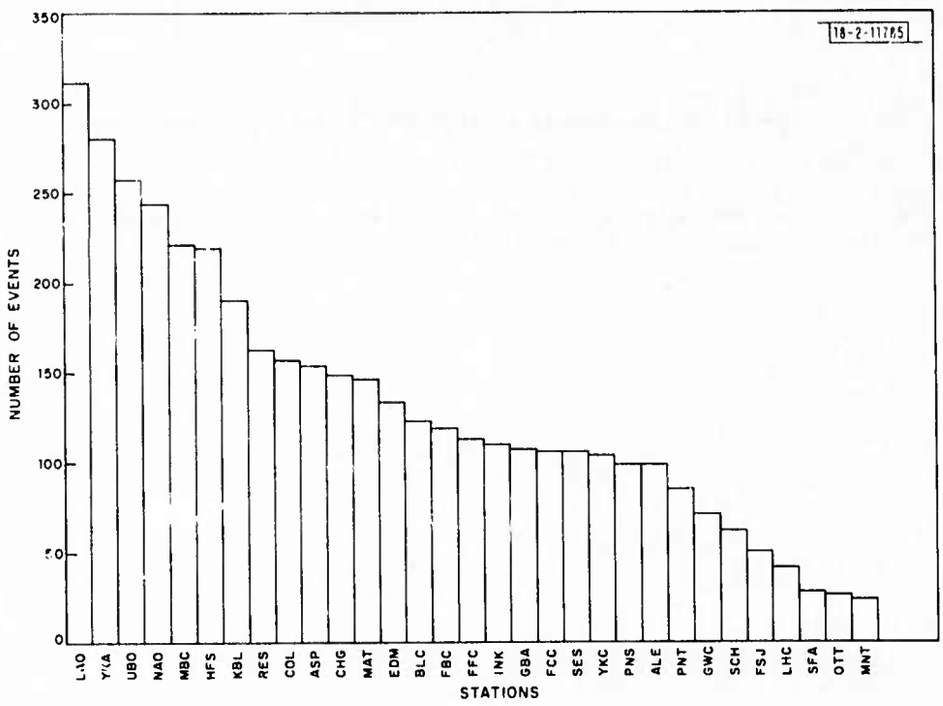

Fig. 1-3. ISM event detections at selected stations.

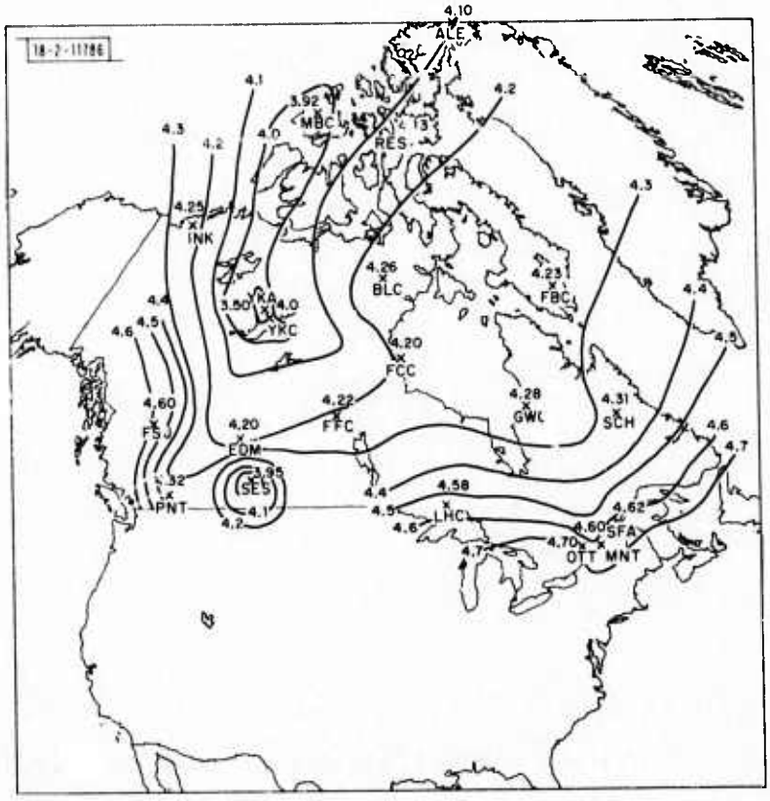

Fig. 1-4. ISM magnitude detection levels for Canadian network.

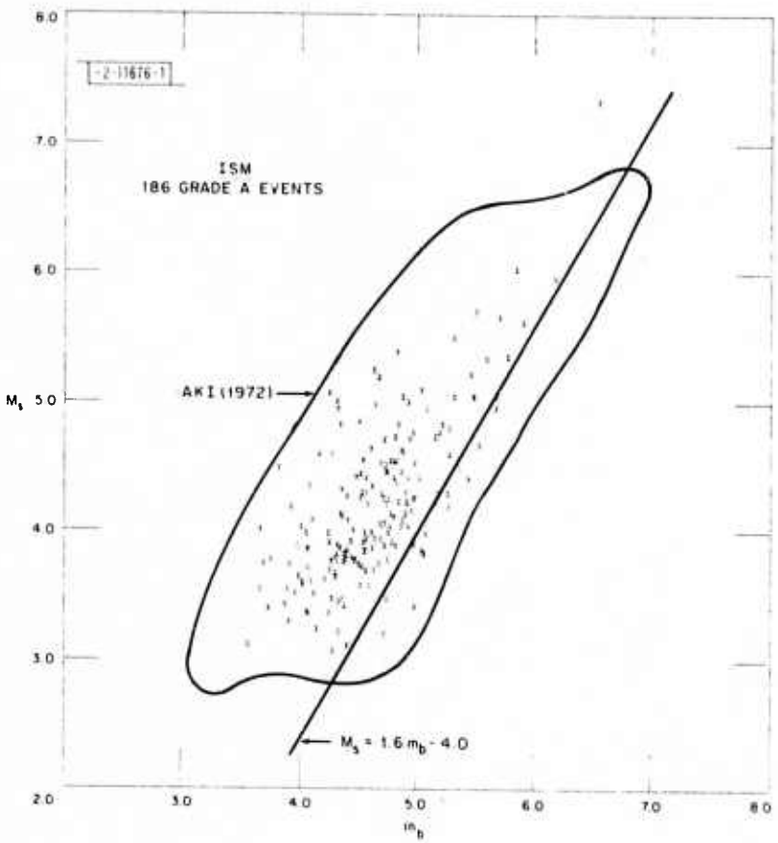

Fig. I-5. Comparison of ISM M_s-m_b data with Aki's summary curve and Gutenberg-Richter line.

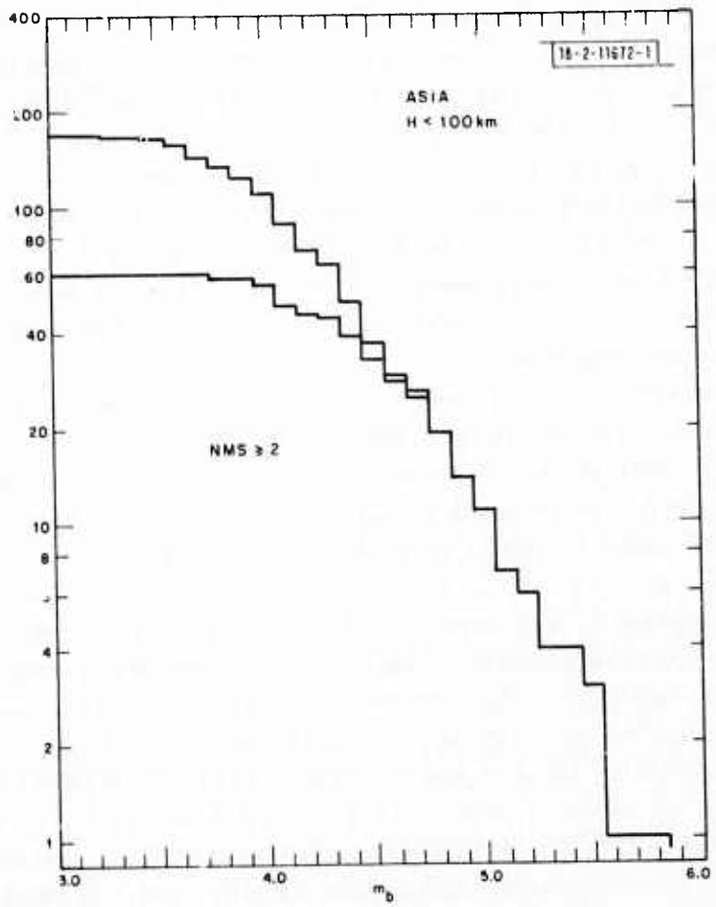

Fig. I-6. Upper line, cumulative distribution of shallow Asian events. Lower line, distribution of these events assigned an M_s based on two or more measurements.

GLOBAL SEISMIC DATA MANAGEMENT SYSTEM

The DARPA NMRO has initiated a major global seismic data collection and utilization project. This project involves the deployment of additional seismic instrumentation; acquisition of digital data in real time and via tape recordings; the analysis of such data to obtain event lists and to test discriminants and operational methods; and the organization, storage, retrieval, and use of raw and processed data in research programs directed toward improving the U.S. seismic discrimination capabilities. In the sequel, we will refer to the system which is going to be realized as the Integrated World-Wide Seismic System (IWWSS). The design and implementation of IWWSS is a complex program requiring careful coordination to achieve a timely and effective working system whose characteristics have been optimized toward the solution of the remaining seismic problems related to discrimination. To this end, Lincoln has started working closely with NMRO, other Government agencies, and contractors to be certain that the system will be seismically valid and useful and that there is good coordination and communication between participants and subsystems.

We discussed the global seismic data project at length with NMRO and participants in the project to obtain from each his concept of the system and related information. Emphasis was on the kind and quantity of seismic data and the overall flow and management of the data. An overview of the system which is evolving was prepared and discussed with participants to be certain that there were no major discrepancies or misunderstandings.

One major component of the IWWSS will be a mass store device for processed and unprocessed seismic data. A working document has been prepared which characterizes the major files to be stored, the logical relationships between these files and other IWWSS components, and the data flow into and between these files. This document and considerable other information has been entered into the On-Line System which is discussed below.

Lincoln has started to use the On-Line System, NLS, developed by Stanford Research Institute, as a working tool for the construction of a directory that will eventually contain considerable information about the IWWSS. The NLS is supported by the TENEX system at Office-1 on the ARPA network. The directory itself will contain many files, each of which will be concerned with specific topics of the integrated world-wide system. One file, OVERVIEW, will contain a general description of the system and system components. Within that file there will be link references (an NLS feature) to more specific documents which will contain more detailed information. There will probably be links throughout all documents to specific and more detailed descriptions of the areas of interest. When the directory is completed, an ARPANET user will be able to view a general description of the IWWSS and then be able to jump to more detailed descriptions and continue to quickly cross-examine the information available. Only a small amount of experience with NLS will be necessary to perform a cross-examination of the available documents. Hopefully, this system and directory will provide system developers, and eventually users, with a rapid access to descriptions of current concepts, processors, software, hardware, organizations, and people involved in the IWWSS.

A tentative skeleton of the file OVERVIEW is nearly completed, along with the definition of several other supporting files. Generally, the first NLS statement in each file will be a table of contents of that file, while the second NLS statement will contain all the links that were cited

within the file. The table of contents is provided so that general references to the file via links from other documents can supply the user with a quick look at the contents of the file. The link references cited within a file will be contained in the second statement of that file so that if there should be any structural alterations of a cited document, then it will be easy to find and change the citations that refer to an altered document. The document characterizing major files on the mass store, which was discussed above, is currently part of this OVERVIEW file.

Our use of NLS is itself a research activity. The system has been designed to facilitate a variety of knowledge-based activities but has had, up to the present time, limited application outside of the immediate community of developers. Nevertheless, we anticipate that it will be of substantial utility for the development, management, and, eventually, final documentation of IWWSS. For this to be true, the seismic user community shortly will need to be expanded beyond the current Lincoln use. We are currently organizing the seismic information within NLS so that we may expand the user group and establish closer dialogs and coordination. In the end, the contents and structure of the NLS files ideally will be the result of mutual activities by various participants.

R. T. Lacoss
R. M. Sheppard

III. EARTHQUAKE SOURCE MECHANISMS

A. FREQUENCY-MAGNITUDE CURVES AND THE M_s-m_b RELATIONSHIP

Frequency-magnitude curves potentially contain some valuable information that has application to the construction of source mechanism theories. Figure III-1 shows the frequency-m_b and frequency-M_s plots for two fairly comprehensive world-wide data sets.

The m_b data have been obtained from the PDE listing of earthquakes (produced by USCGS, NOAA, and USGS) for the years 1964 to 1973. Subsets of this data set show similar features to those shown, and we therefore presume that the effects of changes of organization and definition of m_b are not serious. The resulting plot is clearly a curve, and not a straight line, as is usually assumed. If a straight line is passed through the data in the range $5 \leqslant m_b \leqslant 6$, as shown, it has a b-value of 1.35, which is very high, but agrees with the results of Evernden.[1]

The events recorded during the ISM also may be plotted in terms of frequency-m_b. The resulting curve is parallel to the PDE data at magnitudes greater than 5, but shows a divergence at $m_b \leqslant 5$. If the two curves are matched for $m_b \geqslant 5$ (to allow for slight variations in total activity), the points marked by a cross on Fig. III-1 show the ISM data. The trend indicated by the straight line appears to continue below $m_b = 5$, and since the ISM data were certainly not complete at $m_b = 4.5$, this trend probably continues at least down to $m_b = 4.5$. The discrepancy between the two data sets is presumably the result of incompleteness in the PDE data at magnitudes below $m_b = 5$. There is no evidence that the curve bends over to a smaller b-value in this region, as has been suggested by Evernden.[1]

Because M_s is not assigned to all events in the PDE listing, it is not possible to use this source for a frequency-M_s compilation. The only data set presently available for this purpose is the list of large earthquakes given by Gutenberg and Richter.[2] These data are shown in Fig. III-1, as quoted by Evernden.[1] It is not clear that the magnitudes quoted correspond to recent definitions of M_s, although Evernden[1] suggests that any differences are minor.

The b-value for the frequency-M_s curve is 0.92, in good agreement with many studies on smaller earthquakes (mostly based on local magnitude M_L). It appears that both M_L and M_s provide a consistent measure of seismic moment for magnitudes up to about 7.5. Above this level, the effect of corner frequency is felt, and Gutenberg and Richter's data suggest that the frequency-M_s curve becomes vertical in the vicinity of $M_s = 8.5$. M_s values (based on 20-sec-period waves) should seldom exceed this value, regardless of seismic moment. This result is in general agreement with source mechanism theory.[3]

The slope of the m_b curve indicates that m_b is not a consistent measure of seismic moment for the range of the data shown, $m_b \geqslant 4.5$. At some value of m_b the frequency-m_b curve should turn over to a slope of about 0.9, but it is not yet clear where this occurs. There is no evidence available to suggest that this occurs at $m_b > 4$. At its upper end, the frequency-m_b curve falls off. As in the case of the M_s data, this is due to a corner frequency effect, and the curve appears to become vertical at $m_b \sim 6.7$. m_b values larger than about 6.5 are likely to be extremely questionable.

Although there are some problems in attempting to compare the two curves in Fig. III-1, because they were drawn from different sets of earthquakes, it is possible to use them to discuss the general form of the world average M_s-m_b relation. Clearly, this will be a straight line for $4.5 \leqslant m_b \leqslant 6$, with a slope that is easily calculated to be 1.43. At its upper end, for $m_b > 6$, the corner frequency effect causes the M_s-m_b curve to rise toward the vertical.

An M_s-m_b relation derived directly from the two curves in Fig. III-1 is shown in Fig. III-2. Possible differences in the definition of M_s could move this curve up or down. Note, however, that it shows good agreement with the overall scatter in M_s-m_b observations quoted by Aki,[3] and with the ISM data given by Filson.[4] Slightly better agreement occurs if the curve is raised by 0.2 unit of M_s, and this is confirmed by what PDE data are available (data not shown).

The Gutenberg-Richter relation

$$M_s = 1.59\, m_b - 3.97$$

is a very poor fit to the data, and should be abandoned. A reasonable fit to the curve in Fig. III-2, moved vertically up by 0.2 unit, is given by

$$M_s = 2.91 - 0.68\, m_b + 0.215\, m_b^2 \qquad \text{for } 4.5 \leqslant m_b \leqslant 6.5 \quad .$$

Until more M_s data are available, this relation should be considered as a useful approximation to the world average M_s-m_b relationship. Significant departures from this expression are to be expected within limited geographical regions.

M. A. Chinnery
R. G. North

B. THE MOMENT-M_s RELATIONSHIP, AND THE FREQUENCY OF LARGE EARTHQUAKES

Estimates of seismic moment are now available for a large number of earthquakes. We have selected these data for events with a reliable value of M_s. These are either published PDE M_s values, where a considerable number of stations were used in the determination, or M_s values determined directly from the spectral amplitudes of surface waves as the moment was determined. A compilation of 91 M_o-M_s pairs is shown in Fig. III-3, and includes all reliable events for $M_s > 5$.

The shape of the M_o-M_s relation provides another valuable constraint for source mechanism theories, and it is therefore of interest to attempt to use the data points to define a mean relationship. First we note that the data define a remarkably straight line, when the three largest moment values are omitted. This line has the equation

$$\log M_o = 16.29 + 1.5\, M_s \qquad (5 \leqslant M_s \leqslant 8) \quad .$$

This line is a considerably better fit to the data than the ω^2 model of Aki[3] which is also shown in Fig. III-3.

The upper end of this curve is of considerable interest, although it is only poorly defined by the present data. We expect a corner frequency effect to dominate at some magnitude, and the M_o-M_s curve to trend toward the vertical. The data suggest the presence of this trend, but do not define it clearly.

One unusual approach to this data set is suggested by the frequency-M_s curve shown in Fig. III-4. Can the departure of the frequency-M_s curve from a straight line (at $M_s \geqslant 8$) be attributed entirely to a corner frequency effect? If so, this would imply that the frequency-moment relation should be a straight line. Such a suggestion has been made by Wyss,[5] although he gives no justification for the hypothesis.

We can reverse the argument as follows: Suppose that the frequency-moment graph is a straight line, what is the implied moment-M_s relationship? Clearly, the moment-M_s relation

must be a straight line up to $M_s \sim 8$, and it will then curve upward. The solid line in Fig. III-3 shows such a relationship, and the corresponding frequency-moment relation is shown in Fig. III-4.

Although some uncertainties in the M_s values used in Gutenberg and Richter's data remain, we appear to be able to draw the following conclusions:

(1) The available data are entirely consistent with the hypothesis that the frequency-moment relation is a straight line out to, and probably beyond, $M_o = 10^{30}$ dyne-cm, and that the effect of corner frequency starts to affect M_s determinations (20-sec period) at just about $M_s = 8.0$. M_s values of greater than 8.5 are probably unreliable for any earthquake.

(2) The fall-off in frequency of large earthquakes defined by M_s, for $M_s > 8$, has been used as an argument that earthquakes with source dimensions larger than those commonly attributed to $M_s = 8.5$ are impossible (see, for example, the arguments of Housner[6]). The frequency-moment curve in Fig. III-4 shows clearly that there is no foundation for this argument. It is possible that extremely large earthquakes ($M_o > 10^{30}$ dyne-cm) occur from time to time, particularly on a geological time scale. Although there may be a maximum possible moment, it is apparently beyond the range of presently available data. The whole concept of the "maximum possible earthquake," as commonly used in earthquake risk studies, is very questionable.

M.A. Chinnery
R.G. North

C. DISTORTION OF APPARENT EARTHQUAKE FOCAL MECHANISM BY MANTLE STRUCTURE BENEATH OCEAN RIDGES

Normal-faulting earthquakes on the crests of midocean ridges show an unusual characteristic which has been noted only in passing in the literature: Well-constrained fault-plane solutions derived from P-wave first motions indicate an apparent nonorthogonality of the nodal planes when standard projections are used to map observations back to the focal hemisphere. A particularly clear example of this phenomenon for first-motion data for a ridge-crest earthquake is shown in Fig. III-5(a-b). This earthquake, which occurred on 20 September 1969 on the Reykjanes ridge, is obviously a normal-faulting event. The angle between the nodal planes in the dilatational "quadrant" is only about 60°, however. Two orthogonal fault planes could not be fit to the data without violating a large number of them.

It is our contention that the nonorthogonality of the nodal planes is an artifact of the projection used to map the earth's surface back to the focal sphere. Specifically, the standard tables of ray parameter, or angle of incidence, vs epicentral distance are inadequate when the source region is laterally heterogeneous. We cannot conclusively rule out the possibility that the nonorthogonality is real, e.g., that the earthquake source is best represented by a double couple and a superposed explosive component. An explosive component with P-wave amplitude equal to 0.3 to 0.5 times the maximum P-wave amplitude from the double couple would yield the observed angle of 60° to 70° between the best fitting nodal planes. In particular, a source consisting of a double couple and a superposed explosive component with amplitude about half the maximum double-couple amplitude is entirely consistent with the first-motion data in Fig. III-6. Because of the clear evidence for faulting in the rugged, blocky topography of the mid-Atlantic ridge,

however, we prefer a simple dislocation model for the earthquake mechanism and we attribute the observed nonorthogonality of nodal planes to a path effect.

We have thus constructed models of the upper mantle beneath spreading ridges based upon theoretically calculated temperature fields and experimentally determined phase relationships for peridotite, and have used three-dimensional ray-tracing techniques to calculate the paths of P-waves through these models. Figure III-6 shows examples of such ray paths, which can be seen to be bent downward by a region of very low seismic velocity beneath the ridge axis associated with extensive melting at temperatures above the dry solidus of peridotite. The results of these calculations can easily explain the observed anomalous focal mechanisms, as shown by the corrected data of Fig. III-5(b).

This work is currently being extended to include data on shear wave polarization, which we hope will be able to conclusively differentiate between source effects and path effects.

B. R. Julian
S. Solomon

D. SOURCE DIMENSIONS OF EVENTS IN WESTERN TURKEY

A detailed study has been made of the seismicity of Western Turkey and the mechanisms of some of the larger events in this area, here defined as that part of the country west of 32°E, determined. It has been suggested (McKenzie[7]) that the extensional nature of the deformation here, geologically well evidenced by a series of horst and graben structures, results from the motion of an Aegean plate southwestward away from a Turkish plate, itself moving rapidly westward with respect to Eurasia. In recent years, this region has experienced a number of large and destructive earthquakes, the greatest of which was that of Gediz on 28 March 1970.

All events reported in this area for 1964-70 (ISC bulletin) and 1971-72 (Earthquake Data Reports of the USGS) have been relocated using a program by Julian.[8] The larger, well-located events were used to define a set of station corrections which, apart from the closer stations, appear to vary little across the area considered. These corrections were then used in a "joint epicentre determination" method[9] to obtain relative locations of the smaller events. The relocated epicenters are shown in Fig. III-7. The aftershock sequences of the 1967 (Mudurnu), 1969, 1970 (Gediz), and 1971 earthquakes are clearly seen.

A study of the aftershocks for the 1967 event reveals clearly a westward migration of the shocks with time. This is in agreement with the westward progression of larger events along the North Anatolian Fault (at the westernmost end of which this event occurred) first noticed by Ketin.[10] The aftershock sequence for the Gediz event, the largest in this area in the last five years, is shown in Fig. III-8. The trend of the aftershock distribution agrees well with that of both the fault-plane solution determined by McKenzie[7] and the surface faulting (Ambraseys and Tchalenko[11]). Its length is somewhat greater than that of the latter, and the distribution shown yields an area of faulting of surface dimensions 80 × 40 km. Since both the nodal planes of the fault-plane solution dip at ~45°, the actual area is closer to 80 × 60 km.

For the events of 1967, 1969, and 1971, the aftershocks define the area of faulting much less clearly. Tentative estimates are 70 × 30, 50 × 20, and 40 × 20 km, respectively. The first agrees well with a length of surface faulting of 80 km (Ambraseys and Zatopek[12]).

The seismic moments of 10 events in this region prior to 1971 have been determined from the amplitude spectra of Rayleigh waves.[13] The fault-plane solutions for the events of 1971-72

are virtually identical, viz. normal faulting striking 100° to 120°E of N, with those of 1969-70 (McKenzie, personal communication). The seismic moments for the former can thus be quickly estimated by measuring maximum amplitudes of Rayleigh waves at a number of stations and comparing these amplitudes with those for an event for which the moment is already well determined, in this case that of 28 March 1970.

The source parameters for 16 events in Western Turkey are given in Table III-1. The m_b values quoted are those of the USCGS, and the M_s values are from various sources. The seismic moment M_o and its standard deviation are given in units of 10^{24} dyne-cm, together with the number of station records N used in its determination. For these events for which it has been possible to estimate the length L and width W of faulting, we may estimate the mean relative displacement $\bar{u}$ taking place, through the definition of seismic moment $M_o = \mu \bar{u} A$, where μ is taken as 3×10^{11} dyne/cm^2, and A is the area of the fault plane.

TABLE III-1

EVENTS IN WESTERN TURKEY FOR WHICH THE SEISMIC MOMENT M_o HAS BEEN DETERMINED

Date	Latitude (°N)	Longitude (°E)	m_b	M_s	M_o	N	L (km)	W (km)	$\bar{u}$ (cm)
6/10/64	40.40	28.87	5.9	6.7 MOS	180 ± 70	13			
13/6/65	37.89	29.74	5.1	5.5 MOS	8.2 ± 2.6	6			
22/7/67	40.73	30.86	6.0	7.1 CGS	1500 ± 860	14	70	30	80
5/12/68	36.63	37.07	5.4	6.1 ATH	18 ± 7.5	9			
23/3/69	39.24	28.67	5.6	6.0 MOS	9.1 ± 4.9	15			
25/3/69	39.16	28.52	5.5	6.0 MOS	19 ± 9.2	19			
28/3/69	38.86	28.56	5.9	6.5 MOS	120 ± 67	16	50	20	40
28/3/70	39.20	29.57	6.0	7.0 MOS	300 ± 96	10	80	60	20
16/4/70	39.15	30.24	5.4	5.2 MOS	4.4 ± 0.9	7			
23/4/70	39.45	28.95	5.2	5.3 MOS	3.8 ± 2.7	6			
12/5/71 (06:25)	37.68	29.81	5.5	5.9 CGS	26 ± 13	13	40	20	11
12/5/71 (10:10)	37.45	30.13	5.5		3.5 ± 1	14			
12/5/71 (12:57)	37.61	29.71	5.4	5.2 CGS	10 ± 3	14			
25/5/71	39.20	29.85	5.8	5.5 CGS	12 ± 4	13			
14/3/72	38.79	31.46	5.4	4.9 CGS	3.4 ± 1.7	8			

Brune's[14] method for computing seismic slip from summed moment values in a particular fault zone yields a value of 1.3 cm/year for the extension in Western Turkey over 1964-73. This constitutes reasonably good agreement with McKenzie's[7] estimate of 2 to 3 cm/year for the relative plate motions. Although creep appears to contribute most of the slip in other parts of the Mediterranean and Middle East,[13] in Western Turkey (at least over the last ten years) it seems to have been taking place in earthquakes.

R. G. North

REFERENCES

1. J. F. Evernden, "Study of Regional Seismicity and Associated Problems," Bull. Seismol. Soc. Am. 60, 393 (1970).
2. B. Gutenberg and C. F. Richter, Seismicity of the Earth and Associated Phenomena (Princeton University Press, Princeton, New Jersey, 1949).
3. K. Aki, "Scaling Law of Earthquake Source Time-Function," Geophys. J. R. Astr. Soc. 31, 3 (1972).
4. J. R. Filson, "Long Period Results from the International Seismic Month," Technical Note 1974-15, Lincoln Laboratory, M.I.T. (4 March 1974), DDC AD-776089/5.
5. M. Wyss, "Towards an Understanding of the Earthquake Frequency Distribution," Geophys. J. R. Astr. Soc. 31, 341 (1973).
6. G. W. Housner, "Design Spectrum," in Earthquake Engineering, Chapter 5, edited by R. L. Wiegel (Prentice-Hall, New York, 1970).
7. D. P. McKenzie, "Active Tectonics of the Mediterranean Region," Geophys. J. R. Astr. Soc. 30, 109 (1972).
8. Seismic Discrimination SATS, Lincoln Laboratory, M.I.T. (30 June 1973). Sec. I, DDC AD-766559/9.
9. A. Douglas, "Joint Epicentre Determination," Nature 215, 47 (1967).
10. I. Ketin, "Uber die Tektonischmechanischen Folgerungen aus den Grossen Anatolischen Erdbeben des Letzten Dezenniums," Geol. Rundschau 36, 77 (1948).
11. N. N. Ambraseys and J. S. Tchalenko, "Seismotectonic Aspects of the Gediz, Turkey, Earthquake of March 1970," Geophys. J. R. Astr. Soc. 30, 229 (1972).
12. N. N. Ambraseys and A. Zatopek, "The Mudurnu Valley, West Anatolia, Earthquake of 1967 July 22," Bull. Seismol. Soc. Am. 59, 521 (1969).
13. R. G. North, "Seismic Source Parameters," Ph. D. Thesis, University of Cambridge (November 1973).
14. J. N. Brune, "Seismic Moment, Seismicity, and Rate of Slip Along Major Fault Zones," J. Geophys. Res. 73, 777 (1968).

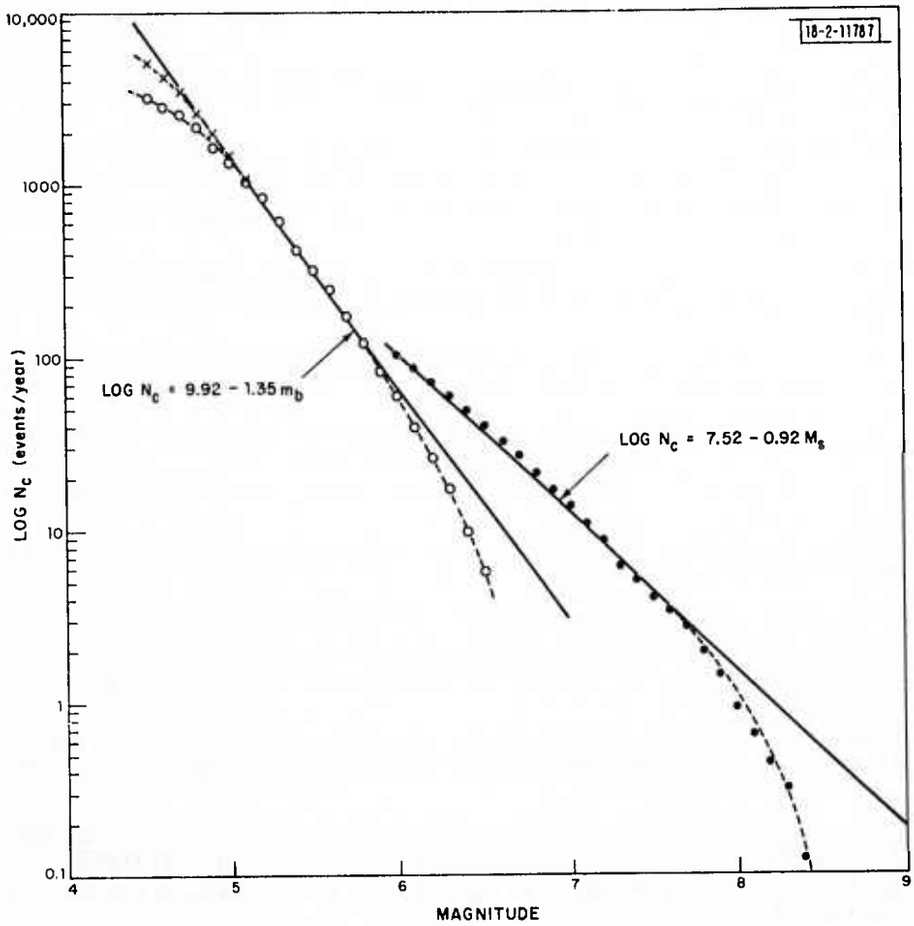

Fig. III-1. Frequency-magnitude curves. Open circles are m_b data from PDE listings; crosses indicate m_b data from ISM; and solid circles show M_s data (see Evernden[1]).

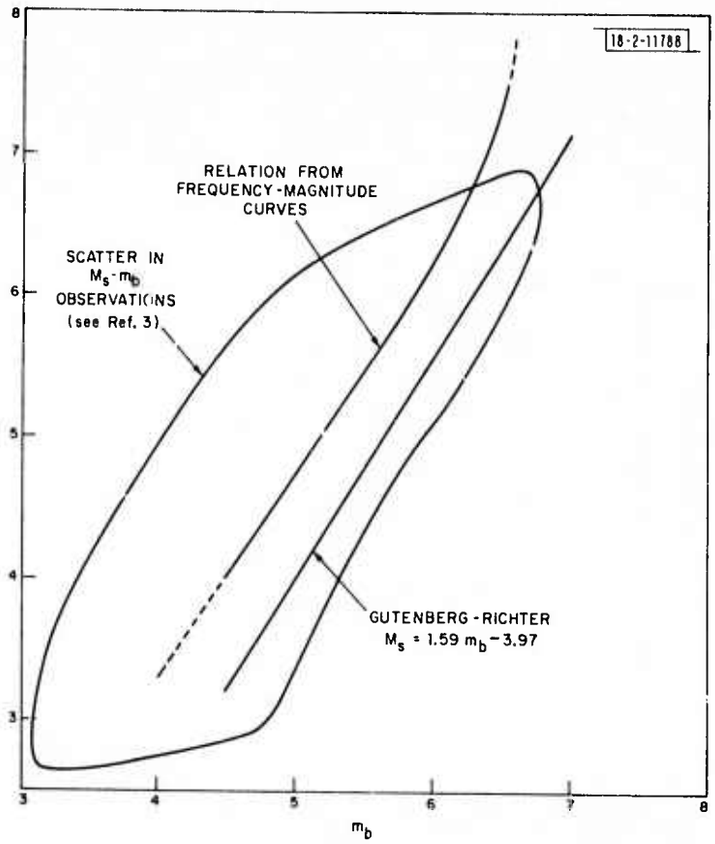

Fig. III-2. M_S-m_b relationships.

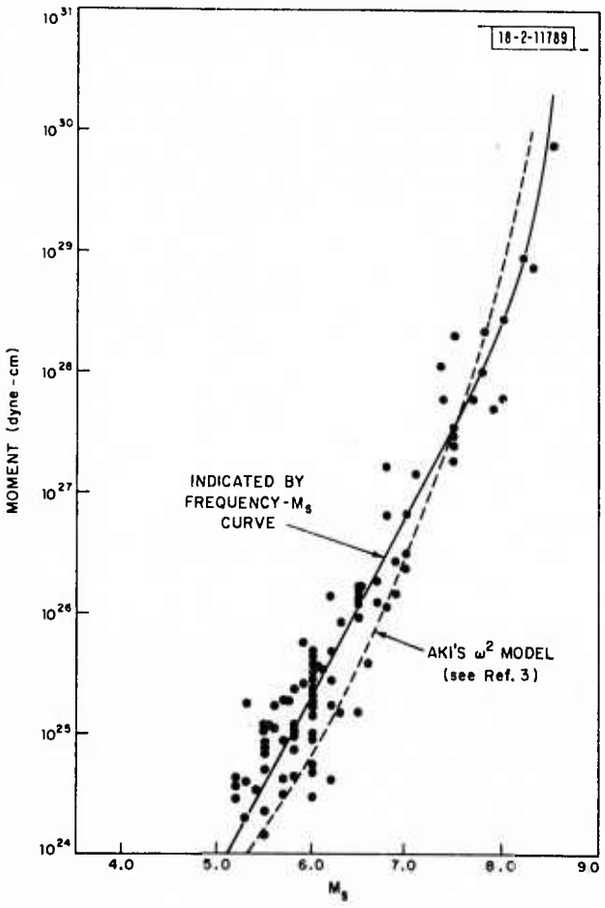

Fig. III-3. Compilation of moment-M_S data for 91 earthquakes with $M_S > 5$. Data shown have reliable M_S value, and have been obtained from numerous published sources. Data in range $5 \leq M_S \leq 8$ are remarkably linear (see text). Solid line is formulated as assumption that frequency-moment graph is straight line (see Fig. III-4).

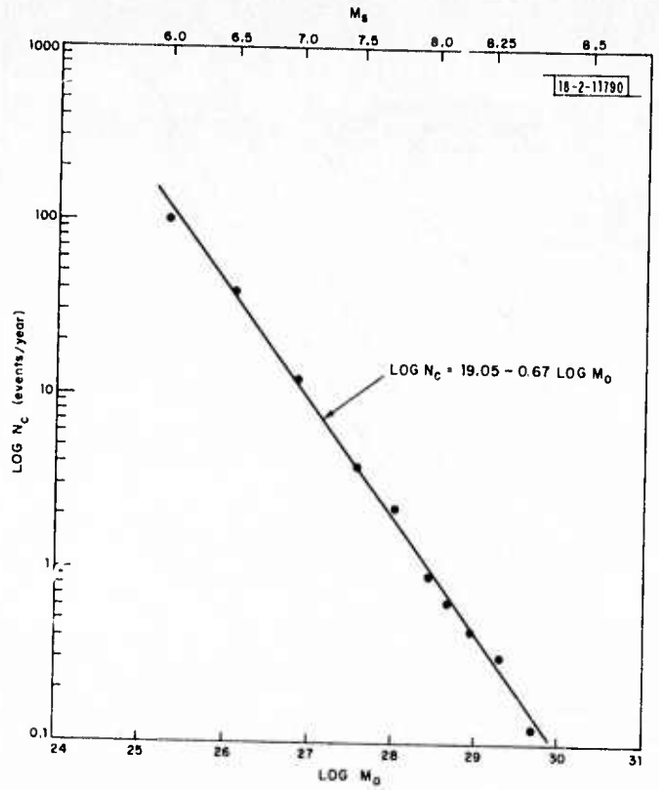

Fig. III-4. Frequency-moment graph that results from substituting moment-M_s relation shown by solid line in Fig. III-3 into Gutenberg-Richter frequency-M_s data shown in Fig. III-1.

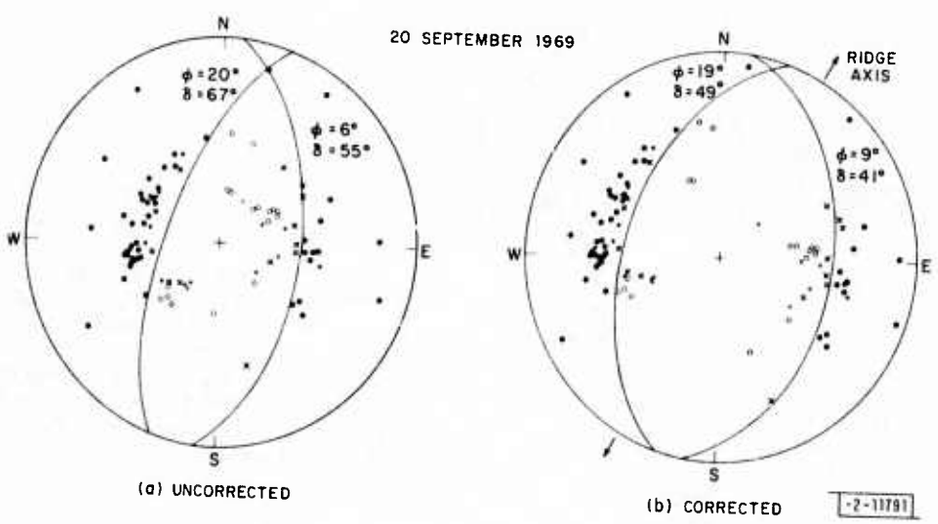

Fig. III-5. (a) Conventional fault-plane solution from P-wave first motions for earthquake of 20 September 1969 (equal area projection). Open circles are dilatations, closed circles are compressions, and circles with superposed crosses indicate probable proximity to a nodal plane. Smaller symbols represent somewhat less reliable readings than larger ones. All data were read from long-period records of WWSSN or Canadian network. Strike φ and dip δ of implied nodal planes are also given. Angle between nodal planes is 60°. (b) Same first-motion data corrected for propagation through ocean-ridge mantle model discussed in text. New fault-plane solution has orthogonal nodal planes.

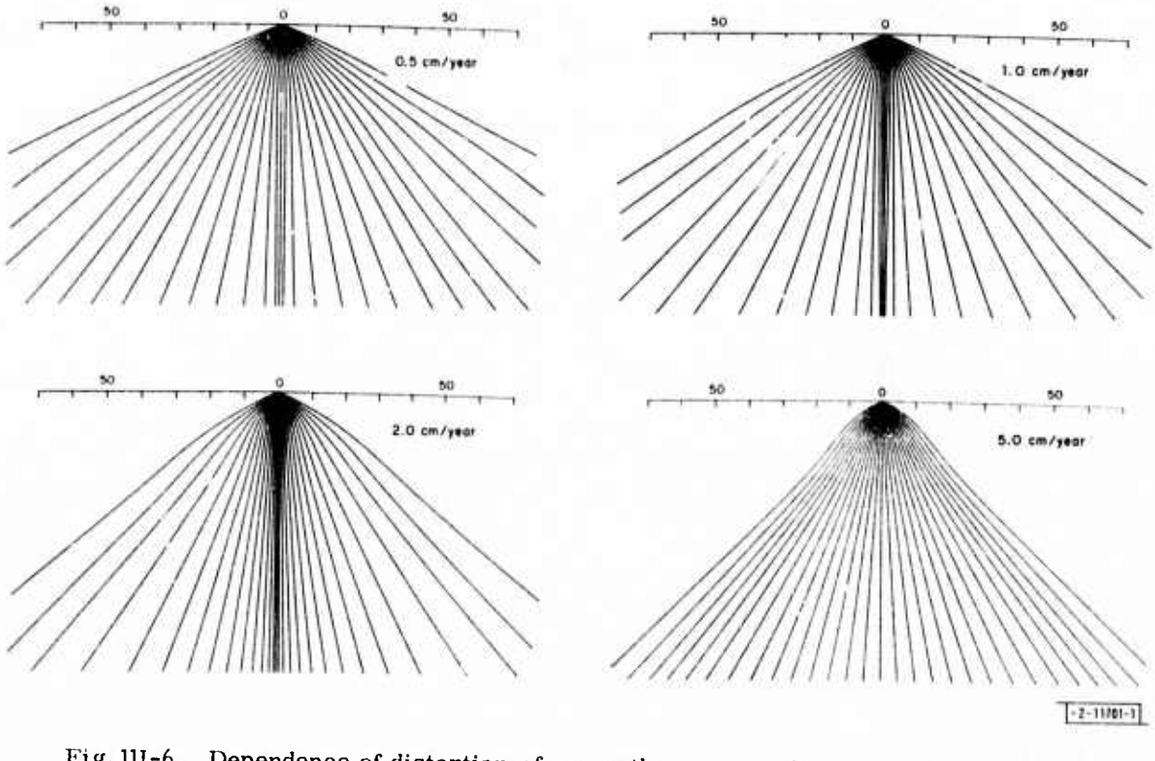

Fig. III-6. Dependence of distortion of ray paths on spreading rate. All ray paths are from surface events on ridge axes. All rays remain in vertical plane perpendicular to ridge axis. Distances along earth's surface are marked in kilometers; no vertical exaggeration. Rays are spaced by 5° in initial takeoff angle, from 0° to ±70°.

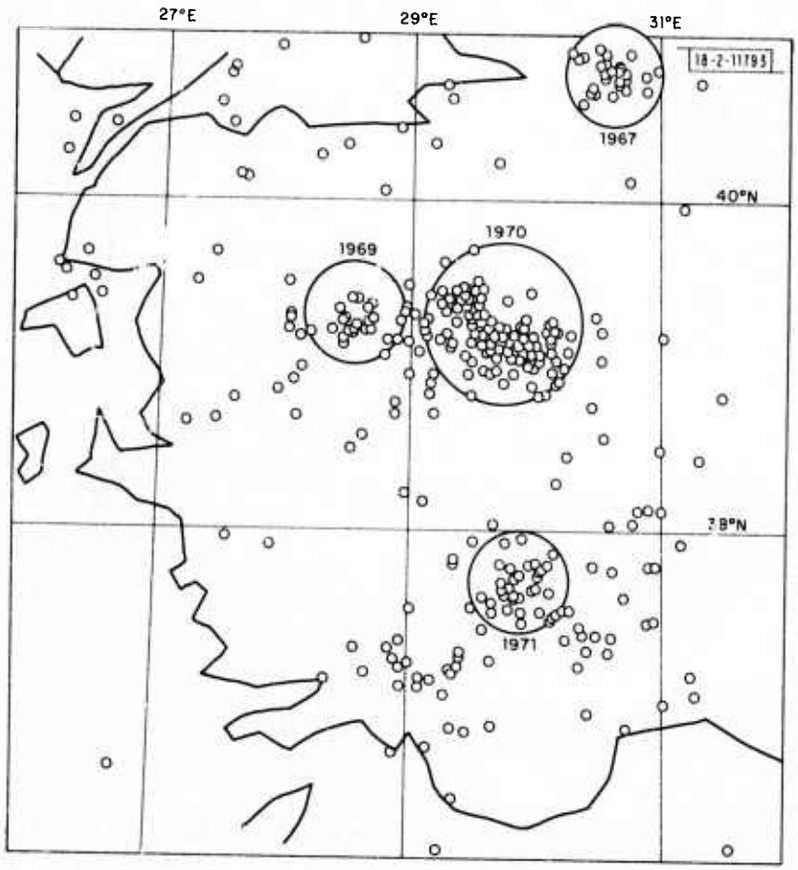

Fig. III-7. Relocated seismicity of Western Turkey for 1964-73.

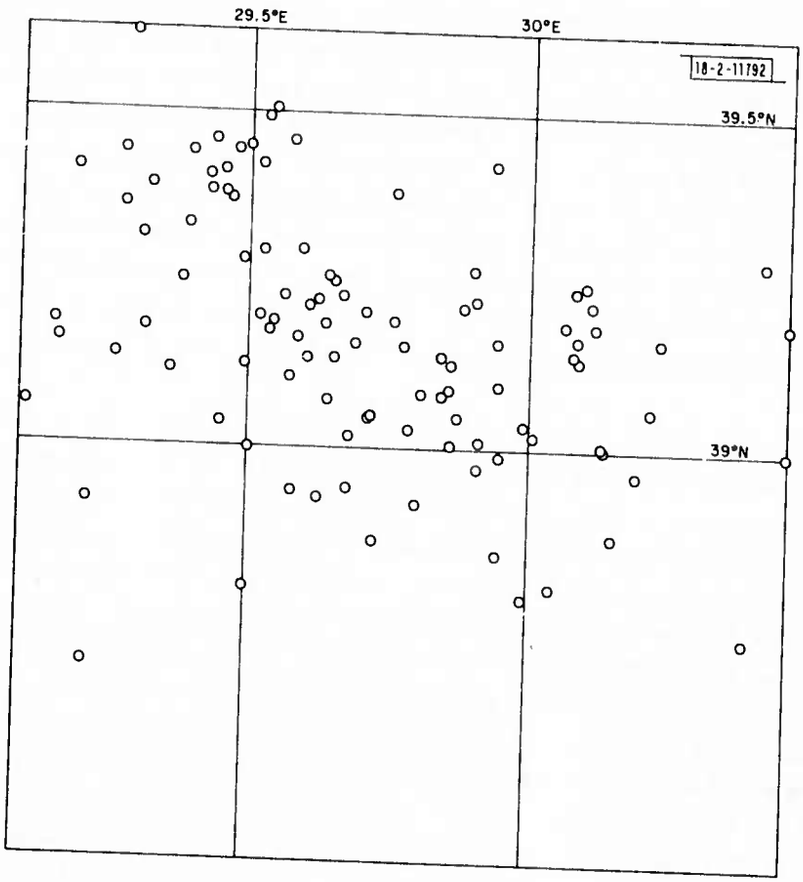

Fig. III-8. Aftershock sequence of Gediż (28 March 1970) earthquake. Relocated epicenters of 146 events for 28 March to 20 June.

IV. FOCAL DEPTH

A. IMPROVED DEPTH-PHASE IDENTIFICATION VIA MAXIMUM ENTROPY CEPSTRAL ANALYSIS

The shape of the waveform and early coda contained in the first few seconds of the short-period seismogram may be determined not only by the direct P-wave but also by multipathed P-waves, by near-source and receiver reverberation, and, in the case of shallow events, by the depth phases. The contribution of each of these secondary arrivals may be nearly the same as that of the direct wave. Knowledge of the onset time and shape of the later arrivals (and, consequently, their removal) is often necessary to obtain an accurate representation of the source function in the short-period band. Determination of the delay time of pP provides the most accurate value for hypocentral depth. Assuming that these secondary arrivals differ in spectral shape from the direct arrival by only a scale factor and an amount due to differential attenuation, their detection may be accomplished by cepstral analysis. Since such echoes arrive in the narrow waveform of the primary signal, the log spectrum contains only a short data sample of the harmonics that peak the cepstrum at the onset time of the echo. Burg's Maximum Entropy (M. E.) prediction error spectral estimator has been used to obtain the necessary resolution.

The value of using the M. E. method for computing the power spectrum of truncated real sinusoids has been demonstrated by Ulrych.[1] In cepstral analysis, the harmonics are complex and of the form $\exp[\mathrm{sqrt}(-1) * \omega/\omega_0]$. The remarkable resolution obtained by using Burg's technique is shown in Fig. IV-1. The 6-point complex M. E. prediction error operator was constructed using 2 cycles of the complex harmonic plus 50-percent white noise. The operator was evaluated around the unit circle (at 10 times the sampling interval). The resulting spectrum plotted on a log scale shows the narrow, well-defined peak. The results are just as good for data segments as short as one-third of a cycle and with as much as 100-percent white noise.

Use of the M. E. technique in cepstral analysis is illustrated in Fig. IV-2. The input seismograms are composed of a source function added to itself after scaling by $-1/2$ and delaying by 0.4 sec. The source functions are the impulse response of the LASA short-period instrument convolved with attenuated impulses with travel time to Q ratios (t*) of 0.25 and 0. The log spectrum was obtained using the fast Fourier transform. The phase (imaginary part of the log spectrum) was unwrapped and a linear component removed. The log spectrum of the instrument was subtracted in the band (0.5 to 6 Hz) where sufficient energy exists to keep the phase well-defined. An 8-point complex M. E. prediction error operator was constructed on the resulting complex frequency series. The power spectra estimated from the operators show well-defined peaks detecting the echoes that are not apparent in the seismograms.

This study is continuing with the application of the method to real data.

T. E. Landers

B. FOCAL DEPTH FROM SURFACE WAVES

In recent years, considerable attention has been paid to the possibility of using surface-wave spectra to determine the focal depth of earthquakes. This method has obvious application to discrimination in the case of shallow events for which depth phases are unavailable and would be useful, even if it could only be shown that the focal depth were likely to be in excess of, for example, 10 km.

Surface-wave spectra depend in a complicated manner upon the source mechanism, focal depth, and elastic parameters of the earth. Studies to determine the focal depth from such information[2,3] generally involve some form of fitting scheme to observed spectra to determine optimum values of the angles describing the orientation of the fault plane and its depth. However, little attention has been paid to the effect of imperfect knowledge of earth structure on such determinations, and generally a standard continental model such as that of Gutenberg and Bullen has been used. A preliminary study has been made of the dependence of spectral amplitudes of Rayleigh waves on reasonable variations in shear-wave velocity structure. The effect of variable compressional wave velocities and densities is less marked.

Initial studies[4] to determine focal depths from surface waves concentrated on the period range 10 to 50 sec, but subsequent work[2] has shown that waves of periods less than ~20 sec may be unpredictably affected by near-surface variations in Q and should not be used. The amplitudes of shorter-period waves decrease with increasing focal depth, but it is difficult to separate this effect from that of attenuation. For many types of mechanism, however, the theoretical amplitude spectra demonstrate a "hole" at periods which increase with increasing source depth. Unless there are layers of low Q over certain depth ranges (which is certainly the case in oceanic structures where they may be introduced by layers of sediment), such holes will not result from Q-variations. The effect of shear-wave velocity variations on the periods at which holes corresponding to particular source depths occur has thus been chosen as suitable for study.

Crustal structure over a limited area can often be fairly well determined from refraction/reflection experiments, but upper-mantle structure is generally inaccessible by these methods. Normally, upper-mantle structure (50- to 500-km depth) is obtained from surface-wave dispersion curves, whose inversion is nonunique and provides a set of possible models satisfying the data. Some constraints on these models occasionally may be provided, in the case of shear-wave velocity structure, by travel-time data. A recent study[5] of upper-mantle structure under the United States by "hedgehog" inversion of Rayleigh-wave dispersion curves has provided sets of models satisfying such curves determined over paths of 400- to 2000-km length. Rayleigh-wave amplitude spectra for sources of various orientation and depth within these models have been computed, and, even for models which all satisfy the same dispersion data, the variation of the position of the spectral hole with period for a particular source depth is considerable. The models studied to date are those determined by Biswas and Knopoff[5] to satisfy their dispersion curves R-3 (Western U. S.), R-6 (North-Central U. S.), and R-11 (South-Central U. S.). The models vary shear-wave velocities in three layers only, designated a lid, a low-velocity zone, and a layer beneath the LVZ.

In the case of path R-3, the models determined include several with a thin high-velocity (4.6 to 4.95 km/sec) layer just below the Moho. Amplitude spectra for some of these models show spectral holes whose periods are virtually invariant with depth over 15 to 50 km, but some of these structures would almost certainly be excluded by shear-wave travel-time data. Models satisfying paths R-11 and R-6 are more reasonable, but even for these the variation with depth of the period of the spectral hole differs considerably from model to model. For all models for R-11, there is negligible difference between spectra for sources at 40- and 50-km depth, and the amplitude difference could easily be attributed to a difference in seismic moment. For some of the R-6 models, there is a similar lack of distinction between spectra for depths of 30, 40, and 50 km. Spectra for a vertical strike-slip fault, observed at an azimuth of 30° with respect to the fault strike, for depths of 15, 20, 25, 30, 40, and 50 km for Model 25 (R-6) of Biswas

and Knopoff[5] are shown in Fig. IV-3. This model appears to be in no way extreme, and for such a fault the position of the holes does not change with azimuth; thus, more observations would not improve the depth resolution.

In Table IV-1, the period at which the spectral hole occurs is given for a vertical strike-slip fault at various depths in seven models satisfying dispersion curve R-6. If one bears in mind that a spectral hole cannot be observationally resolved to better than a ±2-sec period, it can be seen that a hole at, for example, 36 sec yields a depth of 25 to 50 km. Figure IV-4 shows the upper-mantle shear-wave velocity structure for these seven models.

TABLE IV-1

PERIODS (SECONDS) AT WHICH SPECTRAL HOLE OCCURS FOR A STRIKE-SLIP FAULT AT VARIOUS DEPTHS IN MODEL R-6-25 OF BISWAS AND KNOPOFF

Depth (km)	Model						
	226	23	79	179	25	213	99
	Periods (sec)						
15	20	22	22	21	22	23	21
20	28	28	28	27	28	28	28
25	34	34	33	32	32	32	33
30	36	36	36	36	36	36	35
40	40	38	40	38	36	36	40
50	43	38	40	42	38	36	40

Since for each set of models satisfying a particular dispersion curve Biswas and Knopoff have varied only the upper-mantle structure, and maintained the crustal structure constant, it is not surprising that there is little variation in the period of the hole for depths of 5 to 20 km. However, it is certain that crustal structure is subject to even more variation than that of the upper mantle, and thus the resolution of the method for events shallower than 20 km is probably even poorer than demonstrated here for those in excess of this depth. It is proposed to extend this study to include the effect of variations in crustal shear-wave velocities.

We have shown that even in an area where fairly good data on the structure are available in the form of dispersion curves, the accuracy of the surface-wave method for determination of focal depth is limited. In regions such as Central Asia where the structure is very poorly known, the resolution will deteriorate further, without even taking into account the probability that depth characteristics may be introduced spuriously by propagation effects such as attenuation and multipathing.

R. G. North

REFERENCES

1. T. J. Ulrych, "Maximum Entropy Power Spectrum of Truncated Sinusoids," J. Geophys. Res. 77, 1396 (1972).
2. Y-B. Tsai and W-W. Shen, "Utility of Tsai's Method for Seismic Discrimination," Texas Instruments Report (30 November 1972).
3. D. J. Weidner and K. Aki, "Focal Depth and Mechanism of Mid-Ocean Ridge Earthquakes," J. Geophys. Res. 78, 1818 (1973).
4. Y-B. Tsai and K. Aki, "Precise Focal Depth Determination from Amplitude Spectra of Surface Waves," J. Geophys. Res. 76, 5729 (1970).
5. N. N. Biswas and L. Knopoff, "The Structure of the Upper Mantle Under the United States from Dispersion of Rayleigh Waves," Geophys. J. R. Astr. Soc. 36, 515 (1974).

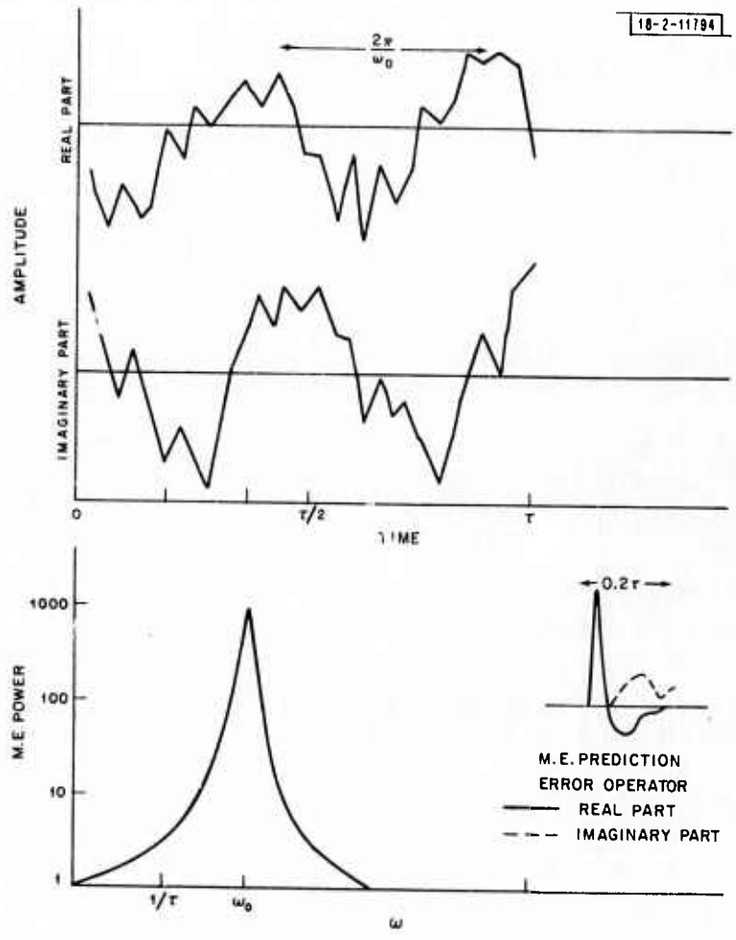

Fig. IV-1. Power spectral estimates computed from 6-point maximum entropy prediction error operator designed on 2 cycles of complex harmonic with 50-percent white noise.

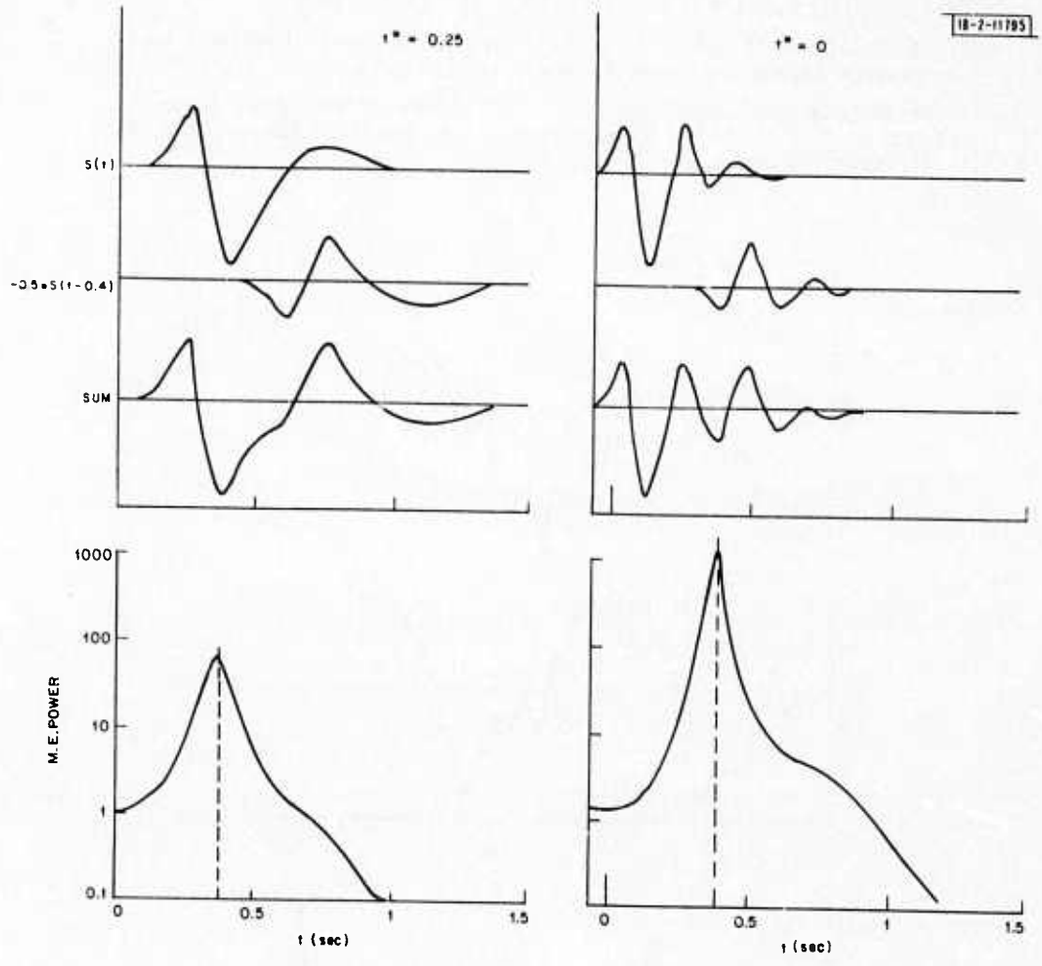

Fig. IV-2. Cepstra computed by Burg's M.E. method for an echo of negative half amplitude at 0.4-sec delay for source waveforms with t* = 0 and t* = 0.25.

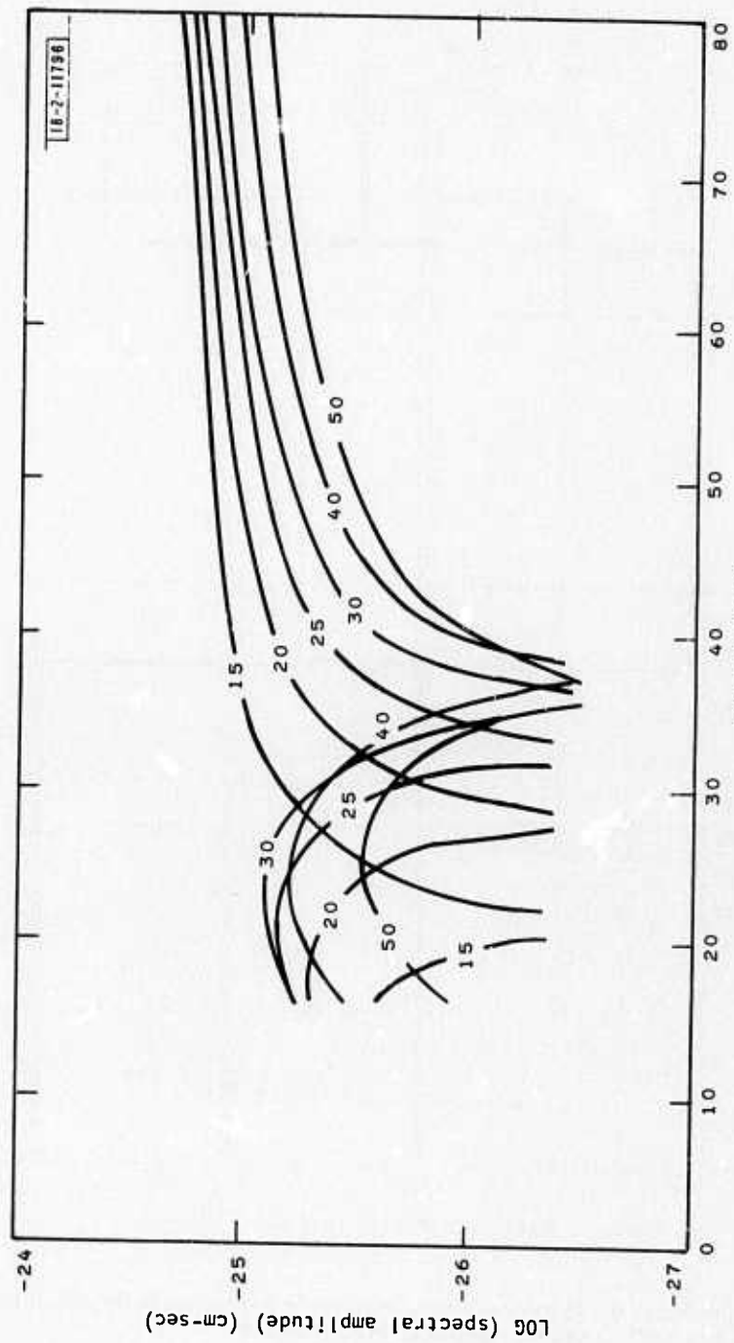

Fig. IV-3. Amplitude spectra for vertical strike-slip fault at depths of 15, 20, 25, 30, 40, and 50 km in Model R-6-25 of Biswas and Knopoff.

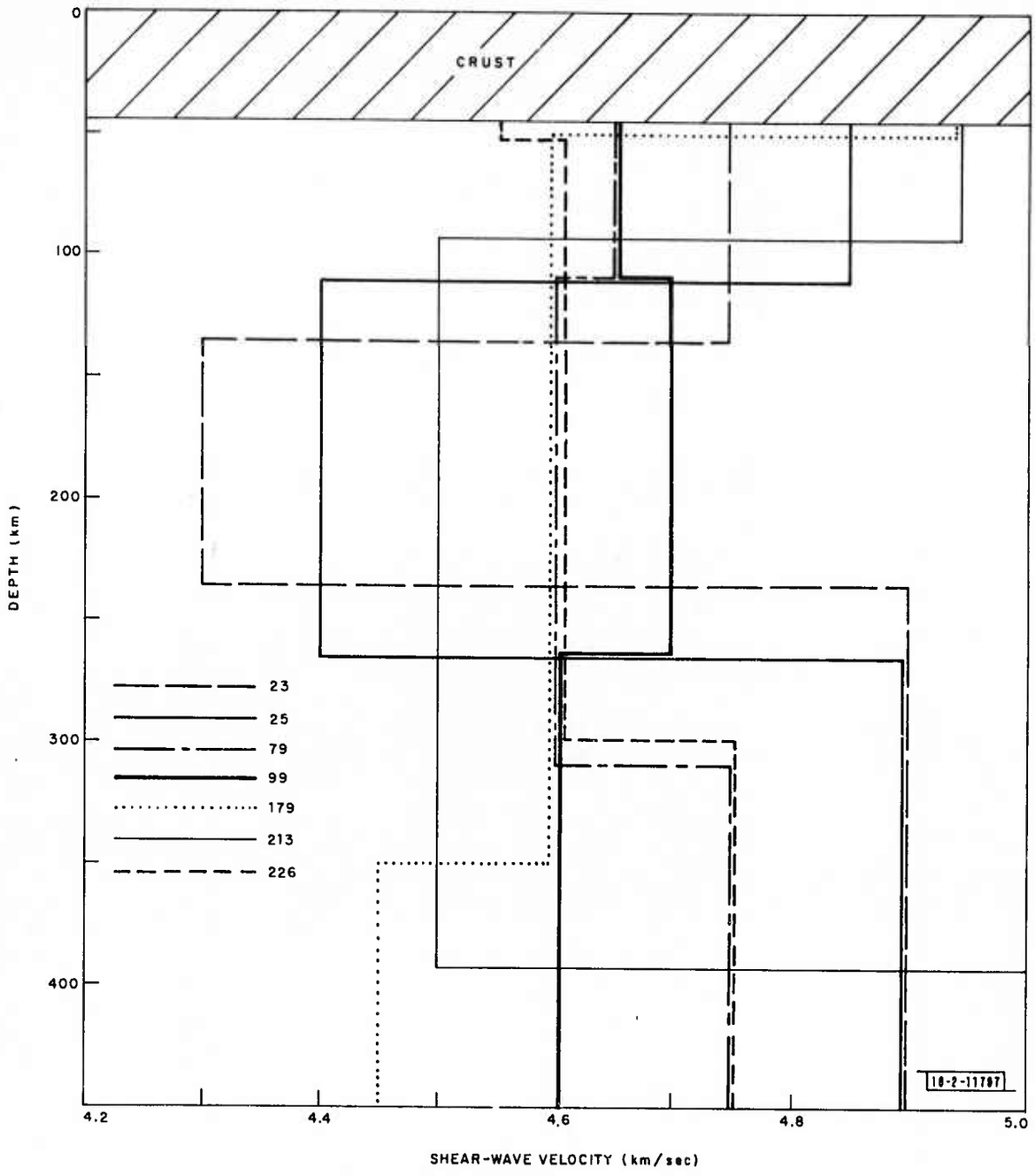

Fig. IV-4. Upper-mantle shear-velocity structure for models determined by Biswas and Knopoff to satisfy dispersion curve R-6.

V. SURFACE-WAVE STUDIES

A. PREDICTING RAYLEIGH-WAVE AMPLITUDES FROM REFRACTION MODELS

Small-scale lateral variations in surface-wave phase velocity cause amplitude and directional anomalies complicating the determination of M_S which is critical in discrimination. In a previous SATS,[1] Julian reported on a phase velocity model for the western U.S. which had some success in predicting angles of incidence. This model has now been extended into the Pacific Ocean and improved through the inclusion of more crustal provinces. Rays traced through this model from LASA or an explosion site show patterns of focusing and defocusing which can be used to predict amplitudes.

Models have been developed for many periods between 15 and 40 sec. The improved phase velocity model (Fig. V-1) shows that 15-sec structures along the Pacific Coast are much more interesting than those well within the continent. Generally, the ocean is about 0.16 km/sec faster at this period, with the transition spread over some 200 km and distorted by local anomalies. The major high in the Oregon area is caused by thin crust under the Columbia Plateau and confirmed by a study of angles of incidence of Rayleigh waves at LASA.

When rays are traced through this model and arrive at LASA, refraction angles of 30° are common, with a maximum of 75° Energy should be focused in coming across the northern California coast and defocused in the Oregon-Washington area. Also, it is apparent that multipathing may begin at the coast, if not before.

As a test of this model, Rayleigh amplitudes at various stations for the Faultless explosion in Nevada were predicted by ray tracing. The separation of adjacent rays is taken to be inversely proportional to the energy concentration in the wavefront. Corresponding data were obtained by reading the maximum vertical long-period displacements from records of WWSSN and LRSM instruments. These data must be corrected for geometrical spreading, instrument response, attenuation, possible double couple source components, and the theoretical source spectrum. The results [Fig. V-2(a-c)] show an accurate prediction of the high amplitudes in the Pacific Northwest and the adjacent lows at Berkeley and Bozeman. Generally, the observed amplitude variations are larger than those predicted, and this is probably because no attempt has yet been made to correct for path-dependent dispersion effects.

Thus, we find that lateral refractions of over 30° must be expected for short-period Rayleigh waves in the western U.S. These should mainly be caused by the structure near the Pacific Coast. Ray tracing with models can predict necessary M_S corrections of up to 0.5 unit which may be important in seismic discrimination.

P. Bird
B. R. Julian

B. RAYLEIGH-WAVE DISPERSION FOR THE INDIAN OCEAN

To gain further understanding of the structural evolution of the oceanic lithosphere, a project involving the study of regionalized Rayleigh-wave dispersion for the Indian Ocean is in progress. The approach of our regionalization is similar to that carried out by Forsyth[2] on the Nasca Plate. In his work, Forsyth used magnetic and bathymetic data in order to partition the spreading lithosphere into lateral age zones. For example, if we model the lithosphere with three oceanic age zones, a suite of dispersion curves for Rayleigh waves traveling through these zones may be used to determine phase velocities within each zone by requiring that the sum of the square of the time

residuals (expected arrival time minus observed arrival time) be a minimum. Furthermore, we may test using statistics whether a particular regionalization model with three age zones is significantly better than a model with just two age zones. For the study on the Nasca Plate, Forsyth's final regionalized model required three oceanic age zones and two continental zones and incorporated anisotropy. It is believed that by studying the Indian Ocean in a similar manner, some important questions about the evolution of very old, oceanic lithosphere may be answered.

To date, our work has concentrated on building up a suitable data base of dispersion curves. Phase velocities for vertical component Rayleigh waves originating on the Mid-Indian Ocean Ridge system have been determined for periods 16 to 150 sec using the single-station technique. This technique requires that the initial phase at the source be known. If the source mechanism and depth for an earthquake are known, we may calculate the initial phase using the theory of Saito.[3] Thirteen events have been studied, and their source mechanisms and depths have been found. From these 13 events, 29 dispersion curves have been computed for the paths shown in Fig. V-3. Total random errors, such as those associated with the uncertainty in origin time, digitization, fault plane solution, etc. result in about 1-percent error in the phase velocity measurements.

We may report various trends in these data. In general, wavetrains from the Indian Ocean are complicated as a result of various interference effects which may be due in part to strong lateral variations in structure which are known to exist in this ocean. Strong attenuation of seismic waves is observed and attributed to thick sedimentary layers. We have tentatively correlated some variations of these "path averaged" data to the age of the ocean floor.

H. Patton

REFERENCES

1. Seismic Discrimination Semiannual Technical Summary, Lincoln Laboratory, M.I.T. (30 June 1973), DDC AD-766559/9.
2. D. W. Forsyth, "Anisotropy and the Structural Evolution of the Oceanic Upper Mantle," Ph. D. Thesis, M.I.T. (September 1973).
3. M. Saito, "Excitation of Free Oscillations and Surface Waves by a Point Source in a Vertically Heterogeneous Earth," J. Geophys. Res. 72, 3689 (1967).

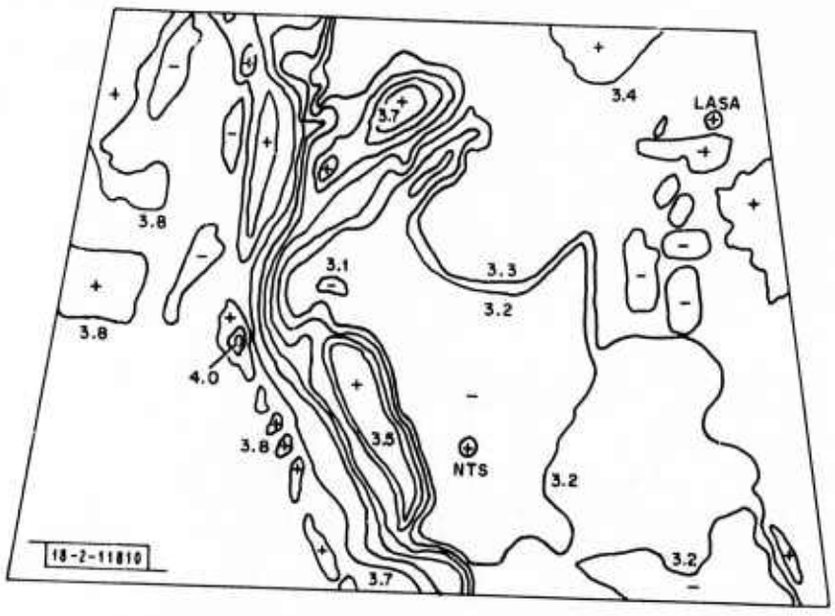

Fig. V-1. Rayleigh-wave phase velocities in kilometers/second at a period of 15 sec predicted from seismic refraction and geologic data.

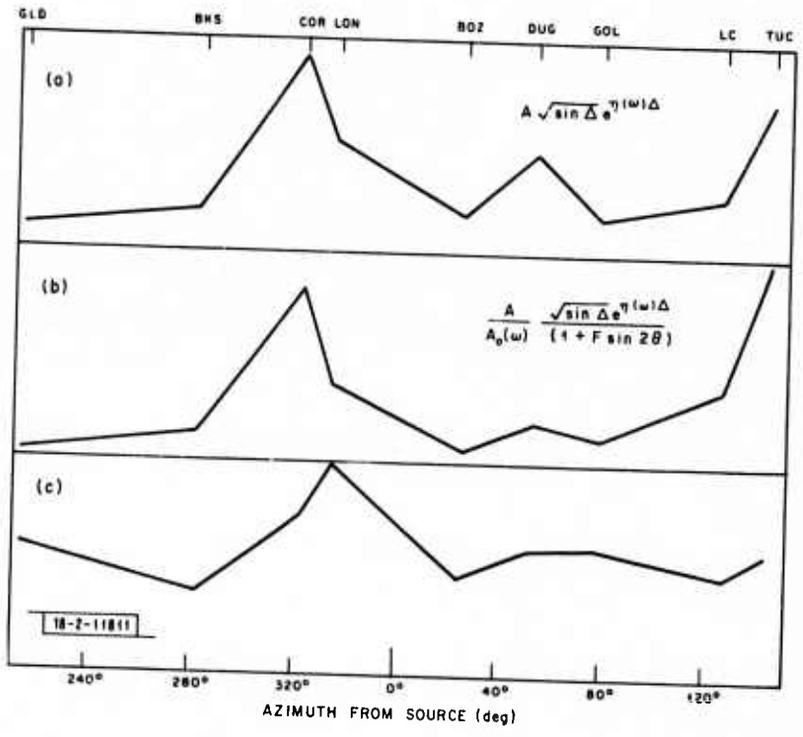

Fig. V-2. Observed and predicted amplitudes of 11- to 16-sec Rayleigh waves from the Faultless explosion in Nevada. (a) Data corrected for attenuation and spreading vs azimuth from the source; (b) same data with source mechanism and source spectrum corrections added; (c) model prediction from ray tracing (T = 15 sec). Base of each graph is at zero amplitude.

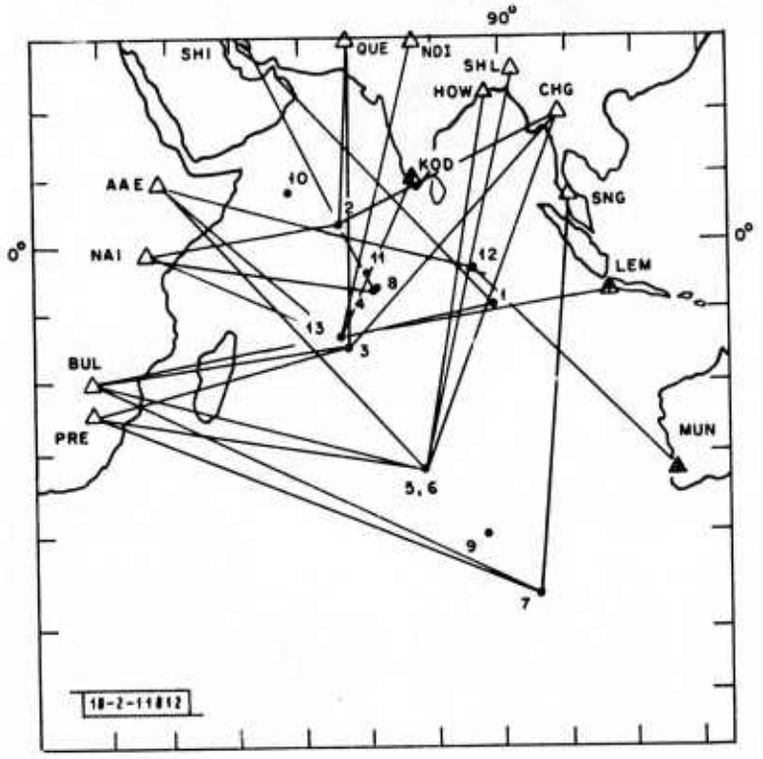

Fig. V-3. Rayleigh-wave dispersion paths in the Indian Ocean.

VI. EARTH HETEROGENEITY

A. AMPLITUDE-DISTANCE CALIBRATION CURVE FROM DEEP FOCUS EARTHQUAKES

The reliability of seismic magnitude determinations is limited ultimately by our ability to correct for the effects of propagation through the earth. Magnitude is conventionally determined from a relationship of the form

$$m_b = \log (A/T) + B(h, \Delta) \qquad \text{(VI-1)}$$

where A is the ground amplitude, T is the corresponding period, h is the focal depth, and Δ is the epicentral distance. $B(h, \Delta)$ is the correction factor for geometrical spreading and attenuation in a spherically symmetric earth. The values of this function given by Gutenberg and Richter[1] are still the accepted standard, although refinements have been proposed by Nuttli[2] and by Booth, Marshall and Young,[3] among others. We propose here another refinement based on some 500 P-amplitude data for 14 deep events in different Benioff zones around the world. The impulsive nature of P-signals from deep focus earthquakes as well as the avoidance of near-source upper-mantle heterogeneity make them well-suited to studying propagation through the lower mantle.

The amplitude data were corrected for instrument response and the effects of reflection/transmission at the free surface, the Moho, and the 650-km discontinuity. Correction for the radiation pattern was also made using fault plane solutions determined from P first-motion data and S-wave polarization angles. All amplitude data requiring a radiation correction in excess of a factor of 3.0 were deleted from the study. A correction for the source spectrum was made assuming that the amplitude spectrum has a corner frequency, below which it is flat and above which it decreases according to a power law. Following Wyss and Molnar,[4] we assumed that for the events in this study, the corner frequencies are above 0.2 Hz, and included only those amplitude data for which the measured periods were greater than 5 sec. The averages of these amplitudes for all events were then used to equalize the moments to a common value. Through a process of iteration, we then determined the average values of amplitude in 2° cells and the station anomalies at different stations.

Figure VI-1 shows our amplitude data, averaged in 2° cells, after correction for station anomalies. These amplitude data roughly correspond to a source depth of 550 km. The solid curve is the ray theoretical amplitude from a model which satisfies the P travel-time data of these deep earthquakes. The sawtooth appearance of ray theoretical amplitude is merely a characteristic of the amplitude calculation from ray theory. The dashed curve is our version of the amplitude distance curve after smoothing the ray theoretical amplitudes to correspond to the data as closely as possible.

Figure VI-2 shows our amplitude-distance curve in comparison with the Gutenberg and Richter[1] curve. The shapes of the two curves differ considerably, possibly due to frequency-dependent attenuation, as the Gutenberg-Richter curve was determined from short-period P-amplitudes whereas our data have periods greater than 5 sec. Incidentally, our curves have more similarity with those determined by Booth, Marshall and Young[3] than with the one determined by Nuttli.[2] Currently, the effect of this curve upon the reliability of m_b determinations is being evaluated.

M. Sengupta
B. R. Julian

B. MORE UPPER-MANTLE REFLECTIONS

In the last SATS,[5] we reported on the observation, at LASA, of intermediate, short-period phases between P and pP from deep earthquakes in western South America. An interpretation that may be given to these phases, which are called pdP, is that they are reflections from boundaries within the upper mantle above these sources; alternate interpretations are that they are aftershocks or reflections from contrasts beneath the array. In order to test these various hypotheses, we have extended the study to other zones where deep seismicity exists. The results of this extension are shown in Fig. VI–3 where the time difference pP-pdP is plotted as a function of distance for the five regions of deep seismicity studied. We point out that a pdP phase is not clear from every deep earthquake studied at LASA, and only the data from unambiguous arrivals are plotted in Fig. VI-3. The solid lines running across that figure represent the depth of source from standard pP-P tables. Although no completely clear pattern is developed, most of the arrivals seem to indicate a depth of the reflection point between 200 and 300 km. Since the upper-mantle structure above these deep sources is complicated by cool lithospheric slabs descending into the mantle, these reflections may not be given to any simple interpretation in terms of plane, horizontal boundaries. There is one rather loose correlation that may be relevant. The seismicity of some of the deep earthquake zones is characterized by a dearth or gap in the activity at intermediate depths, generally between 300 and 500 km. This gap is particularly well-defined beneath South America and the New Hebrides, less so beneath the Sea of Okhotsk, and only vaguely apparent beneath the Bonin and Tonga Islands. In Fig. VI-4, we have plotted the implied reflection depths of these pP precursors along with the extent of the seismicity gaps, if clear, in the five regions studied. From this figure it appears that many of the reflection points fall near the top boundary of the intermediate zones of low or no seismicity. If this correlation is a physical one, it would imply rather sharp changes in the elastic parameters of the upper mantle associated with the upper boundaries of the aseismic zones. Since the pP precursors seem to be fairly common, we can reject the aftershock hypothesis with some confidence. We likewise tend to reject a source beneath the array as a cause of these phases since they are not found following the short-period P-waves of shallow events, however the clarity of such a reflection may depend on the frequency content of the primary wave.

We would like to correct two errors in our previous discussion[5] of these phases. The array traces in Figs. III-8(a) and (b) of Ref. 5 are mislabeled. They should read, from the top, B1, F3, F4, A0, B3, C4, B4, C1, C2, B2, C3, and D3. It has been pointed out to us[6] that the phrase "plane of constant latitude," used in the text[5] and in the caption to Fig. III-10, is not correct. A surface of constant latitude is a cone, not a plane. The seismicity discussed was in fact projected onto the plane of a great circle which dips 25° with respect to the equatorial plane at a direction of 70°W longitude on that plane.

M. Lin
J. R. Filson

C. PRECURSORS TO S AND SKS FROM DEEP FOCUS EARTHQUAKES

LASA data have been searched for arrivals preceding the S- and SKS-phases which are expected to result from the conversion of shear wave energy to compressional wave energy at upper-mantle discontinuities. Numerous authors have used precursors to PP and P'P' in studying such discontinuities. The purpose of this study is to determine the local structure of upper-mantle discontinuities under seismic array sites, information about which could be valuable for many studies involving array data.

The criteria used in identifying a precursor to a main phase are slowness, azimuth, and amplitude. The slowness and azimuth of an arrival are found by picking the arrival time of the phase on as many of the array channels as possible and best fitting a plane wave front. A precursor resulting from the conversion of shear to compressional energy will have the same slowness and azimuth as the main shear arrival. The Velocity Spectral Analysis (VESPA) process is currently being applied to determine the slowness of arrivals preceding the S- and SKS-phases.

Events recorded at LASA having a magnitude of 5.4 or greater and a depth greater than 200 km were selected for this study. S-to-P conversion is expected only beyond critical distances of 82° for the 420-km discontinuity, and 89° for the 670-km discontinuity. Events were selected for this study with distances greater than 89° so that precursors to the S-phase converted at both discontinuities could potentially be seen for each event. The shadow zone due to the core reduces the amplitude of P- and S-phase arrivals for events with distances greater than 102° so that no events with distances greater than 102° were selected.

The S- and SKS-phases were chosen for the study because of their low values of slowness and their arrival in a portion of the record where there are comparatively few arrivals of other phases. The short-period vertical component and the three long-period components were examined for each of the 26 events selected.

Precursors were most commonly seen in the range 60 to 70 sec before the S- and SKS-phase arrivals. The slowness values of the S-phase are quite different from those of the SKS-phase, so that the corresponding main phase of a given precursor can be clearly determined. Precursors were most prominent on the vertical components. Precursors to the S- and SKS-phase arrivals generated at the 670-km discontinuity are expected about 65 sec before the main phase, and for the 420-km discontinuity about 45 sec before the main phase.

The precursors varied from a single peak to a coda of several wavelengths. The period of the precursors averaged around 8 to 10 sec on the long-period data, and around 1 sec on the short-period data.

Figure VI-5 shows a precursor to the S-phase arriving 70 sec before the main phase on long-period channels. A precursor to the SKS-phase is shown in Fig. VI-6 arriving 64 sec before the main phase on short-period channels.

The spectrum of the precursor coda is being analyzed in an effort to gain insight into the detailed structure of the transition zones.

C. T. Bolt
B. R. Julian

D. SCATTERING EFFECTS ON PcP/P AMPLITUDE RATIOS

A strong source of amplitude scattering for short-period data is the crust and upper-mantle structure under the receiver. This is impossible to estimate with a single station; however, an array of closely spaced seismographs gives a clear picture of the complexity of scattering effects. Studies by K. Aki[7] and J. Capon[8] show that a considerable amount of amplitude scattering at LASA can be caused by a medium with small random fluctuations of velocity of a percent or two about the mean.

This has disastrous consequences for studies based on amplitude ratios of short-period phases such as P and PcP. To illustrate this, six events from a recent study[9] were chosen which had good signal-to-noise ratios at all LASA subarrays with distances of 44° to 63° along a narrow azimuthal sector 302° to 317°. Four events were clustered in the region from Andreanof Island to Amchitka Island, and two events were located near Kamchatka. Table VI-1 contains a list of the events used.

TABLE VI-1

PcP/P AMPLITUDE RATIOS FOR SIX EVENTS

Event	Date	Origin Time (GMT)	NOAA Location		Depth (km)	m_b	Distance (deg)	Azimuth (deg)	PcP/P Amplitude Ratio		
									Mean	Standard Error	Standard Error/Mean
1	21 Feb 68	21:07:57	51.4°N	176.0°W	47	5.2	44.4	302.8	0.72	0.40	0.56
2	22 Jun 67	15:36:39	51.7°N	176.8°W	54	5.3	44.7	303.5	0.23	0.10	0.43
3	11 Aug 68	12:37:28	52.1°N	179.9°W	159	5.5	45.4	305.1	0.62	0.25	0.40
4	29 Oct 65	21:00:00	51.4°N	179.2°E	0	6.1	47.1	304.5	0.46	0.20	0.43
5	9 Oct 67	14:10:57	54.1°N	155.1°E	393	5.2	58.3	316.8	0.24	0.13	0.54
6	8 Jan 68	13:50:42	49.1°N	151.3°E	284	5.0	63.3	314.1	0.16	0.05	0.31

PcP/P amplitude ratios were then computed for each subarray. In Table VI-1, the mean PcP/P ratio and standard error across LASA for each event are tabulated. Note that the standard errors decrease with increasing epicentral distance except for event 2. This is deceptive, however, because the mean PcP/P values also decrease with distance. In the last column of Table VI-1, the normalized standard errors, i.e., standard error/mean, seem to be more or less comparable at all distances. These statistics show that PcP/P ratios on subarray beams can easily vary by ±50 percent relative to the mean PcP/P ratio across the LASA.

A measure of similarity of two amplitude patterns is given by their correlation coefficient. The log amplitudes of the P and PcP phases were computed at all 21 subarrays for the six events. The mean of each log amplitude pattern was removed yielding a pattern of positive and negative log amplitudes for each phase. For event K, these can be represented by the vectors

$$\bar{P}^K = \{P_i^K\}$$

and

$$\overline{PcP}^K = \{PcP_i^K\}$$

where i = 1, 21 corresponding to the 21 subarrays of LASA.

The correlation coefficient of $\bar{A}$ and $\bar{B}$ is defined as

$$C(A,B) = \frac{\bar{A}\,\bar{B}}{\sqrt{(\bar{A}\,\bar{A})\ (\bar{B}\,\bar{B})}}$$

Three sets of correlation coefficients were calculated, namely: $C(P^K, PcP^K)$, $C(P^K, P^{K+1})$, and $C(PcP^K, PcP^{K+1})$. The first is the correlation coefficient of P and PcP patterns from event K; the second involves the P patterns from two adjacent events in Table VI-1; and the third coefficient is for PcP patterns from two adjacent events. These calculations are shown in Fig. VI-7.

For the events at distances less than 50°, P and PcP patterns are essentially uncorrelated, whereas at about 60°, the patterns are moderately correlated. On the other hand, PcP patterns from adjacent events are well correlated, as shown by the dashed lines between adjacent event distances, except for the correlation between the events at 47° and 58°, the largest distance gap. The P patterns are slightly less correlated than the PcP patterns, but generally are better than the correlation between P and PcP patterns for each of the adjacent events.

The implication of these data is that P and PcP amplitude patterns at LASA can be duplicated by closely located events, the PcP pattern being more consistent than the P pattern with variations in epicentral distance. This result indicates that the amplitude fluctuations of subarray sum data are dominated by complex transmission and diffraction of the seismic signals by the structure under LASA rather than near the source region or deep in the mantle. Most likely this is the case under many seismograph stations, and suggests that single-site measurements of PcP/P ratios are not reliable for determining parameters of the core mantle boundary.

By forming beams of the P and PcP phases, the incoherent amplitude fluctuations are averaged out, yielding more stable estimates of PcP/P ratios. If the PcP/P ratios measured at different subarrays are assumed to be independent with equal means and variances, then one can expect that the standard errors of PcP/P ratios obtained from the beams are $1/\sqrt{21}$ (~0.22) times the standard errors of the single subarray measurements. From Table VI-1 this implies that the standard errors for each ratio using beamed data are about 10 percent of the mean value, which is a more acceptable standard error.

C. W. Frasier

E. SHORT-PERIOD CODA OF A LOCAL EVENT AT LASA

It is widely accepted that the seismic coda of small local earthquakes is largely due to scattering by inhomogeneitics in the earth's crust, as suggested by Aki.[10] The actual mechanism of this scattering is, as yet, unsatisfactorily explained and must be understood to accurately define those parts of a seismogram due to source effects and those due to path effects.

It is possible to discern at least two processes contributing to codas. The first is strong forward scattering discussed by Chernov.[11] This process has the effect of summing a large number of multipathed signals. Essentially, all the energy in such coda travels along the ray path connecting the source to the receiver. Additionally, as a wave passes a receiver it may be scattered locally by smaller scale inhomogeneities in the vicinity of the receiver. This phenomenon of multiple scattering is the second process contributing to seismic codas. According to the analysis of Howe,[12] which predicts an equipartition of energy between all wavenumbers, the energy in this section of the coda arrives from all directions. A superposition of these two processes may provide a good qualitative description of P-, S-, and surface-wave coda.

Figure VI-8 shows the energy in the frequency band 1.0 to 2.0 Hz of a short-period record at the F2 subarray of LASA for a strip-mining blast 113 km away, as a function of time. The peak energy in this band is due to the arrival of the S-wave. The high-resolution wavenumber spectrum for this section of the record, shown in the figure, indicates that virtually all the energy is arriving from the direction of the blast. The wavenumber spectrum for the later S-coda indicates that energy is arriving from all directions with shear- and surface-wave velocities.

Figure VI-9 shows the local energy in the frequency band 0.2 to 1.0 Hz. In this band, the peak energy occurs at the arrival of the Rayleigh wave. The wavenumber spectrum shows that virtually all the energy in this section of the record arrives from the direction of the source, with a velocity appropriate to 2-sec Rayleigh waves under LASA. The coda of these arrivals produces a wavenumber spectrum that again shows that energy arrives from all directions, with velocities ranging from P- to surface-wave velocities. These results bear out the salient points of the model.

Before this model can be effectively applied to local events and teleseisms, it is necessary to determine more accurately the nature of the P-, S-, and surface-codas. This information can be used to determine values for the correlation distances and turbidity coefficients which characterize the type of scattering in the crust under LASA.

J. Scheimer
T. E. Landers

REFERENCES

1. B. Gutenberg and C. R. Richter, "Magnitude and Energy of Earthquakes," Ann. Geofis. 9, 1 (1956).
2. O. Nuttli, "The Amplitudes of Teleseismic P Waves," Bull. Seismol. Soc. Am. 62, 343 (1972).
3. D. Booth, P. D. Marshall and J. B. Young, "Long and Short Period P Wave Amplitudes from Earthquakes in the Range of 0° – 114° (Preprint).
4. M. Wyss and P. Molnar, "Source Parameters of Intermediate and Deep Focus Earthquakes in the Tonga Arc," Phys. Earth Planet. Interiors 6, 279 (1972).
5. Seismic Discrimination Semiannual Technical Summary, Lincoln Laboratory M.I.T. (31 December 1973), DDC AD-777151.
6. E. Bullard, personal communication.
7. K. Aki, "Scattering of P Waves Under the Montana LASA," J. Geophys. Res. 78, 1334 (1973).
8. J. Capon, "Characterization of Crust and Upper Mantle Structure under LASA as a Random Medium," Bull. Seismol. Soc. Am. 64, 235 (1974).
9. C. Frasier and D. Chowdhury, "Effect of Scattering on PcP/P Amplitude Ratios at LASA from 40° to 84° Distance," submitted to J. Geophys. Res.
10. K. Aki, "Analysis of the Coda of Local Earthquakes as Scattered Waves," J. Geophys. Res. 74, 615 (1969).
11. L. A. Chernov, Wave Propagation in Random Media (McGraw-Hill, New York, 1960).
12. M. S. Howe, "On the Kinetic Theory of Wave Propagation in Random Media," Philos. Trans. R. Soc. Lond. A. 274, 523 (1973).

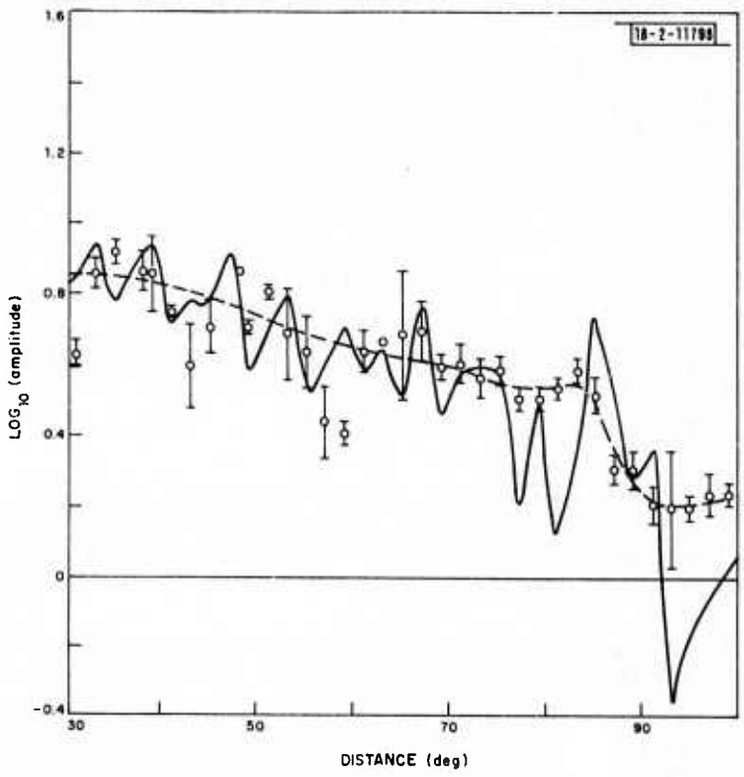

Fig. VI-1. Amplitude-distance curve. Circles are average amplitude (microns) in 2° cells; vertical lines are standard errors of the average; solid line is ray theoretical amplitude from model MKS1(P), satisfying travel-time data from deep focus earthquakes. Note ray theoretical amplitude has been adjusted vertically to satisfy amplitude data. Dashed line is smooth amplitude-distance curve.

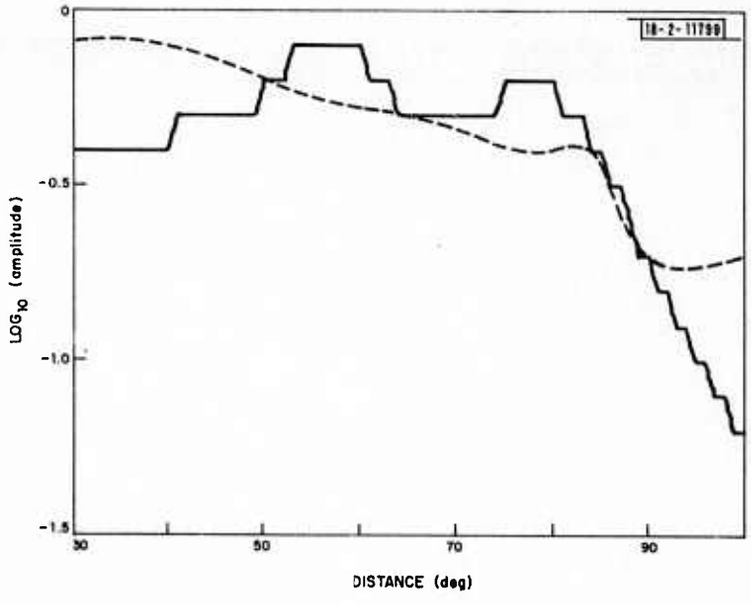

Fig. VI-2. Comparison of amplitude-distance curves. Solid line is amplitudes (microns) of Gutenberg and Richter for earthquake of magnitude 6.0 and period of 1 sec. Dashed line is our version of amplitude-distance curve.

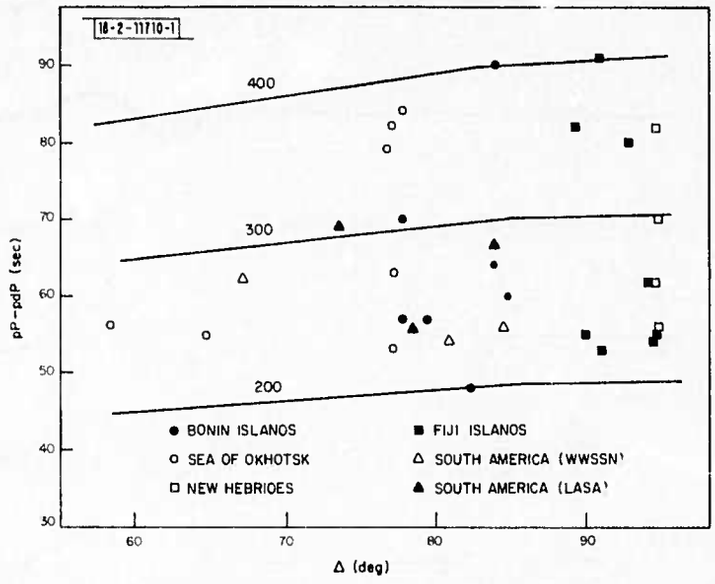

Fig. VI-3. Time interval pP-pdP at LASA from deep sources in various regions. Three solid lines represent depths of reflection points in kilometers.

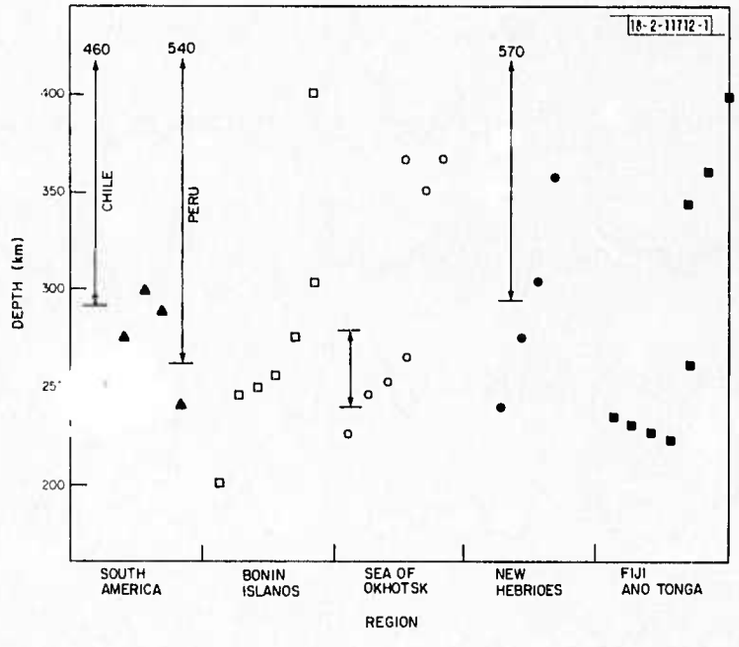

Fig. VI-4. Correlation between implied reflection point depths (points) and seismicity gaps (arrows) in various regions.

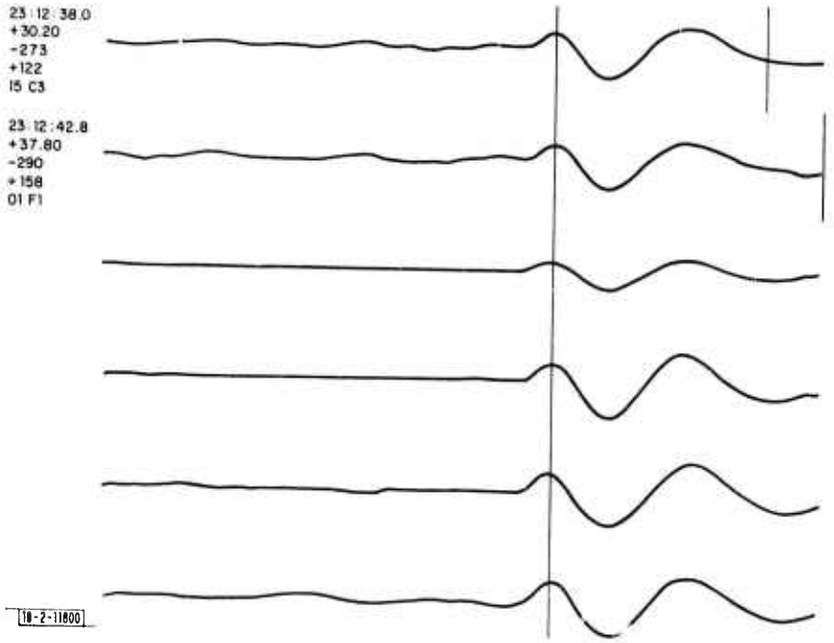

Fig. VI-5. Long-period, subarray sums from LASA showing precursor to S-phase arriving 70 sec before main phase from earthquake occurring on 6 August 1971 at 22h 52m 15s, 530 km deep beneath 20.3°S, 177.8°W.

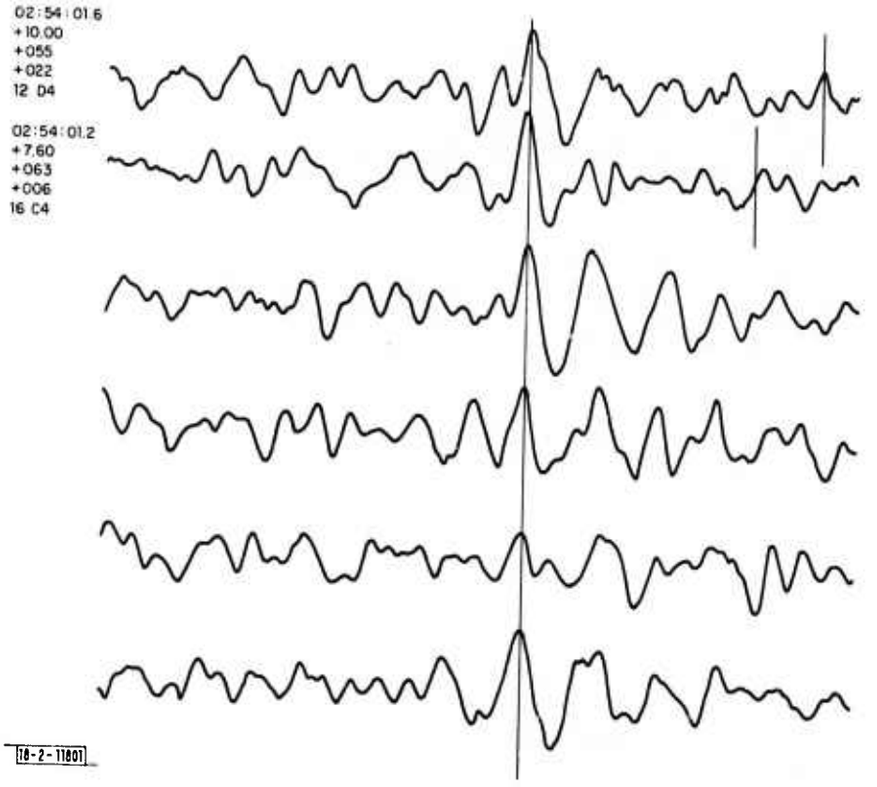

Fig. VI-6. Short-period, subarray sums from LASA showing precursor to SKS-phase arriving 64 sec before main phase from earthquake occurring on 24 January 1969 at 2h 33m 03.5s, 595 km deep beneath 21.9°S, 179.5°W.

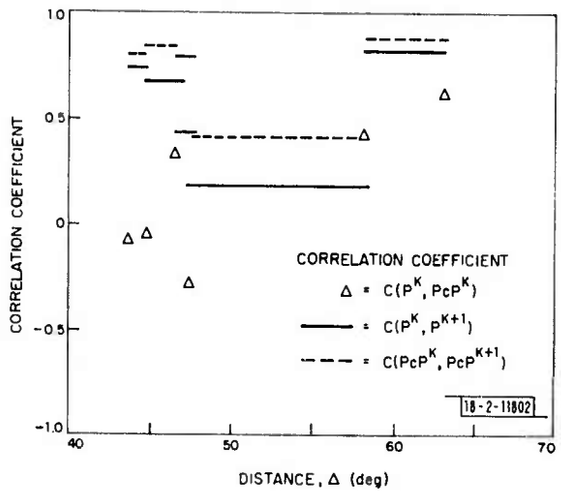

Fig. VI-7. Correlation coefficients of P and PcP patterns of same event at LASA, of P patterns from adjacent events, and PcP patterns from adjacent events.

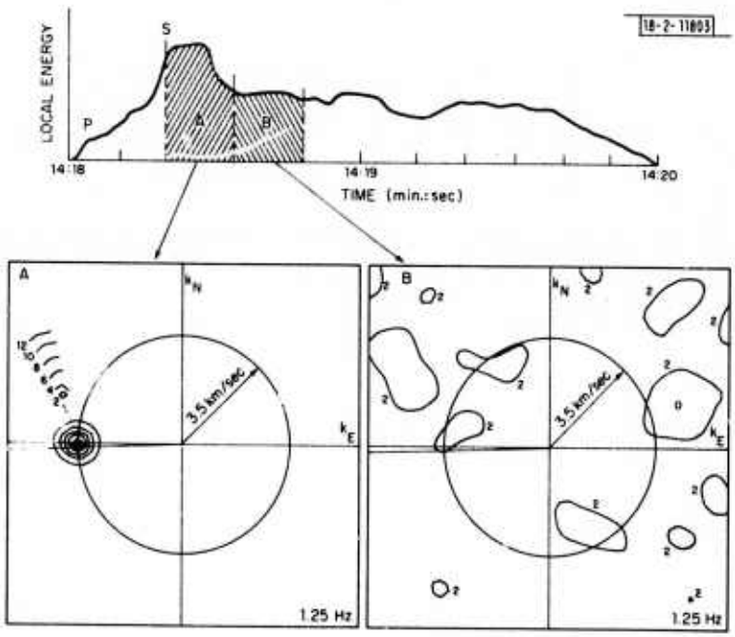

Fig. VI-8. High-resolution spectra for S-arrival and S-coda in frequency band 1.0 to 2.0 Hz for strip-mining blast near LASA.

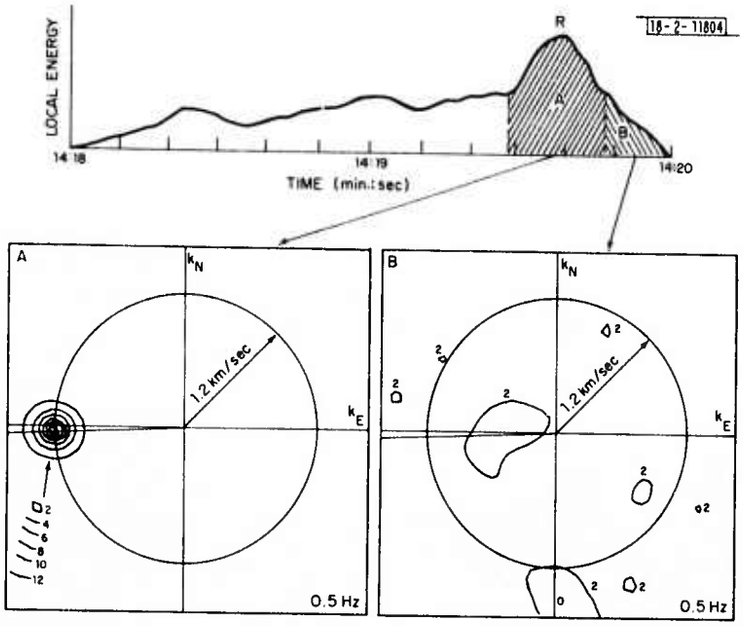

Fig. VI-9. High-resolution spectra for Rayleigh-wave arrival and Rayleigh-wave coda in frequency band 0.2 to 1.0 Hz for same blast in Fig. VI-8.

VII. GENERAL SEISMOLOGY

A. SEISMICITY OF CENTRAL ASIA AND TECTONICS OF THE BAIKAL RIFT ZONE

In two earlier reports[1,2] we presented fault-plane solutions, horizontal slip-vectors, and paleopoles for Central Asia. We also presented a hypothetical plate-model for Central Asia.

Figure VII-1 shows our seismicity map for Central Asia. The seismicity is plotted for the region bounded by 18°N and 58°N and by 60°E and 140°E. Historical as well as instrumental seismicity are plotted on the map. The historical seismicity is obtained from the ARPA seismicity map. The instrumental data until 1961 are also obtained from the ARPA map. Instrumental data from 1962 to 1971 were taken from the PDE cards. All magnitudes are >4.0 (m_b). The epicenters are shallow (<70 km) except a few in the Burma region and those of the Hindukush Zone which are of intermediate depth (between 70 and 300 km). The very deep earthquakes (~500 km) near Korea are interpreted as being due to the Pacific plate dipping down under Asia.

Even though the seismicity in Central Asia is diffused over a wide region, we are still able to identify zones of concentrated seismicity. It is along these zones that the plate boundaries were drawn in Fig. IV-12 of Ref. 2.

The Baikal Rift Zone:- This zone is situated on the boundary of the Siberian Platform and exhibits singular features. We were not able to get enough data to do more than two focal mechanism solutions in the region, since most of the earthquakes between 1963 to 1972 were <5.5. However, Misharina[3] has done fault-plane solutions for these events using data from USSR stations, and has plotted the axes of tension and compression. Some of the faults in the region are shown in Fig. 15 of Ref. 3. All earthquakes in the lake are pure normal. Going from the northeastern end of the lake toward the Stanovoy mountains, the focal mechanisms are still mostly normal but some have a large component of strike slip. Our solutions Nos. 10 and 19 (see Ref. 1) are in this region. No. 10 is pure normal, while No. 19 is strike slip with a small component of thrust, which agrees with Misharina's solutions. But if we move along the main Sayan fault, which extends at an acute angle of 40° to the western flank of the rift zone, and which has no depressions of the rift type, all the focal mechanisms are of purely compressional type. If we move even further along the Siberia-W. China plate boundary (which is discussed later), the solutions are still purely compressional – Solutions 6, 18, 21, and 23. Misharina[3] indicates the region where the sudden change from extension to compression takes place. But below this boundary, the earthquakes within the plate are of pure-strike slip type, with a small component of thrusting in some cases. Solution 14 and the Gobi-Altai earthquake[4] solutions are of this type. The level of seismicity in this region is higher than in the rift zone.

Thus, there is a region of near-horizontal stretching at the upper end of the lake and near-horizontal compression beyond the lower end of the lake. Florensov[5] claims that there are signs of increase of rift depression in width and depth and of active rift structures in the Stanovoy mountains, and that these indicate the continuity of development of the rift zone in the eastern direction. The rift structures, according to Florensov, are along the ancient faults of the Pre-Cambrian and early Paleozoic eras.

The rift zone is characterized by an intense isostatic instability with large negative gravity anomalies which some claim may be as large as −100 mgals!! Borisov[6] is of the opinion that beneath the entire rift is a very deep graben-like structure that goes down into the upper mantle and is filled with crust mantle mixture.

Lubimova[7] has conducted a study of heat-flow data in the lake and on the land surrounding the lake. It is obvious that the Baikal Zone is a region of abnormally high heat flow (the highest value being 3.4 HFU). But the region just beyond the southwest tip of the lake shows lower values. Lubimova and Polyak[8] note this "clear boundary" separating the Baikal Rift Zone from the "relatively uniform field of somewhat lower values in the adjacent part of the Siberian platform, that of the Irkutsk plateau (~1.0 HFU)." Note that the transition from high to low heat-flow values occurs at the exact same spot as the transition from extensional to compressional stresses.

Thus, we find a most unusual phenomenon occurring on the boundary between the Siberian and the W. China plates. There seems to be compression on the part from the Hindukush to the southern tip of Lake Baikal, but from there to the Stanovoy region there is spreading. The W. China plate thus seems to be turning in a clockwise direction relative to the Siberian plate which is assumed fixed, about a point at the southern tip of Lake Baikal.

S. Das

B. PROPAGATION OF THE NORSAR SUBARRAY TIME CORRECTIONS INTO ASEISMIC REGIONS

The analysis of the NORSAR time anomalies has reached its conclusion with the implementation of the subarray time corrections into the Analysis Console System and into various computer programs. Before the corrections were implemented, however, it was necessary to extrapolate the time errors into regions that were aseismic or lacked sufficient data to yield a value for the station correction. The process used for the extrapolation of the data is the same one successfully used earlier on the LASA station corrections for core phases.[9]

The first step in the process is to plot the subarray time errors on a graph of azimuth vs error and a plot of distances vs error. From these two plots, it can be determined what type of function will best approximate the subarray error. In the case of the NORSAR subarrays, the function seemed to have a linear term or a quadratic term with distance and was definitely a three-cycle Fourier series type function with azimuth. A good example of this is subarray 03C and is shown in Fig. VII-2. This generally represents the functional relationship of the NORSAR subarray time anomalies with distance and azimuth. The next step in the procedure was to fit the desired function, in a least-squares sense, to each set of subarray time residuals. The function that was used had 21 coefficients, and the fit resulted in a root-mean-square error that was generally about 0.07 sec. The evaluation of this function at regions that are aseismic will yield a fair value for the subarray station correction in those areas.

However, additional refinement of the functional values was necessary. Since the final corrections were to be stored in the form of a table, the function was evaluated at each cell in the table (cell size is 10° in azimuth by 0.2 sec/deg in $dT/d\Delta$). Where actual data existed at a cell point, it was used rather than the function value; where there was no actual data, the function value was used. The resulting table was then smoothed somewhat to reduce the sharp boundaries between some cells. This final table was then used as the NORSAR subarray correction. A graphic example of the final output for subarray 03C is shown on the polar plot in Fig. VII-3. Here, the radial component is $dT/d\Delta$ starting at 4.0 in the center and extending to 10.0 at the outer circumference.

R. M. Sheppard

C. SINGLE-CHANNEL EVENT DETECTOR IN REAL TIME

In the previous SATS,[2] a single-channel event detector was described which operates in real time on a PDP-7 computer. Here, we present results of using this program on a set of 480 synthetic events derived from 16 real events recorded at NORSAR.

Briefly, the detection scheme compares the spectral power of the seismogram, averaged over a short time window, with the spectral power averaged over a long window preceding the short window. A detection occurs when the short-term power (averaged over several frequencies of interest) exceeds the long-term power (averaged over the same frequencies) by a factor of T, the threshold parameter. When a detection is declared, the long-term average (LTA) is fixed, while the short-term average (STA) is continuously updated in time. As the event coda decays in time, the ratio of STA to LTA decreases until it falls below T, at which time the detector turns off. If no new detections occur within an arbitrary time lag L, then the LTA is updated, and the detection scheme continues.

Experiments have shown[2] that the frequencies 1.0, 1.5, 2.0, and 2.5 Hz were suitable for calculating the STA and LTA for NORSAR data. Other parameters used were a threshold T = 2.5, a lag L = 10 sec, a short-term averaging window of 3.0 sec, and a long-term averaging window of 30 sec.

NORSAR beams of 16 events were formed using the center sensors of the NORSAR subarrays. The events sample different azimuths with distances from 38.3° to 77.8° from NORSAR. Seven minutes of noise from 5 NORSAR channels were selected from 13:02:00 to 13:19:00 GMT on 23 February 1972. The noise channels are 1A0, 1B0, 2B0, 3B0, and 4B0. Each event beam was added to a set of the 5 channels at 1-min. intervals from 13:03 to 13:08, scaled down by a factor of 0.5 or drop in m_b of 0.3 relative to the beam a minute earlier. Thus, from each of the 16 NORSAR events, 30 synthetic events were produced making a total population of 480 synthetic events. Each set of 5 channels was bandpass filtered with a 3-pole Butterworth filter with 3-dB points at 0.8 and 3.5 Hz.

The event detector was run on all 5 channels for each of the events. Figure VII-4 shows a histogram of the results as a function of NORSAR m_b. The shaded area indicates the number of detected events, and the unshaded area denotes the undetected events. These data were used to compute the incremental detection probability for the detection scheme. First, the histogram data were grouped in bins 0.2 magnitude unit wide, then the ratio of detected events to events processed was computed at each magnitude. The results are displayed in Fig. VII-5 where the solid curve is the detection probability for all 5 channels, i.e., using the histogram of Fig. VII-4, and the dashed lines are for the 2 channels showing the largest deviation from the average for detection probabilities >0.5. For all channels together, the 90-percent incremental detection threshold is about $m_b = 4.8$. These results are for a small fixed window of winter noise. The 90-percent threshold would be expected to be a little lower if summer noise data were used.

An application of this program to the problem of multiple events is being studied. In particular, the constant updating of the LTA without a lag after a detection occurs will enable this scheme to automatically detect short-term bursts of energy in the coda of other events.

C. W. Frasier

REFERENCES

1. Seismic Discrimination Semiannual Technical Summary, Lincoln Laboratory, M.I.T. (31 December 1972), DDC AD-757560.
2. Ibid. (31 December 1973), DDC AD-777151.
3. L. A. Misharina, The Stresses in the Earth's Crust in Rift Zones (Nauka, Moscow, 1967).
4. N. A. Florensov and V. P. Solonenko, "The Gobi-Altai Earthquake," translated from Russian by Israel Program for Scientific Translations, Jerusalem (1965).
5. N. A. Florensov, "Rifts of the Baikal Mountain Region," Tectonophysics 8, 443 (1969).
6. A. A. Borisov, Deep Structure of the Territory of the USSR, According to Geophysical Data (Nauka, Moscow, 1965).
7. E. A. Lubimova, "Heat Flow Patterns in Baikal and Other Rift Zones," Tectonophysics 8, 457 (1969).
8. E. A. Lubimova and B. G. Polyak, "Heat Flow Map of Eurasia," in The Earth's Crust and Upper Mantle, edited by P. J. Hart (AGU Geophysical Monograph 13, 1969).
9. Seismic Discrimination Semiannual Technical Summary, Lincoln Laboratory, M.I.T. (31 December 1971), DDC AD-737092.

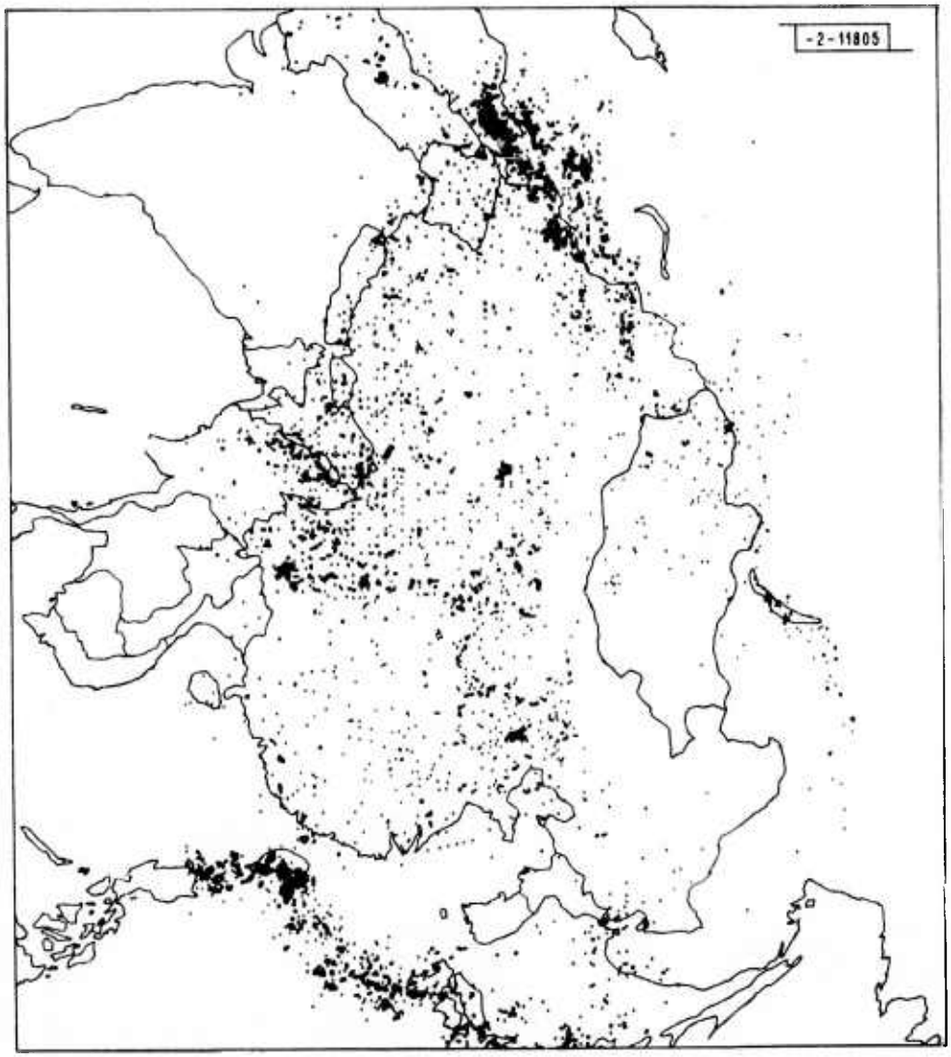

Fig. VII-1. Seismicity of Central Asia in region bounded by latitudes 18°N to 58°N and 60°E to 140°E, until 1971. All magnitudes have $m_b \geq 4.0$.

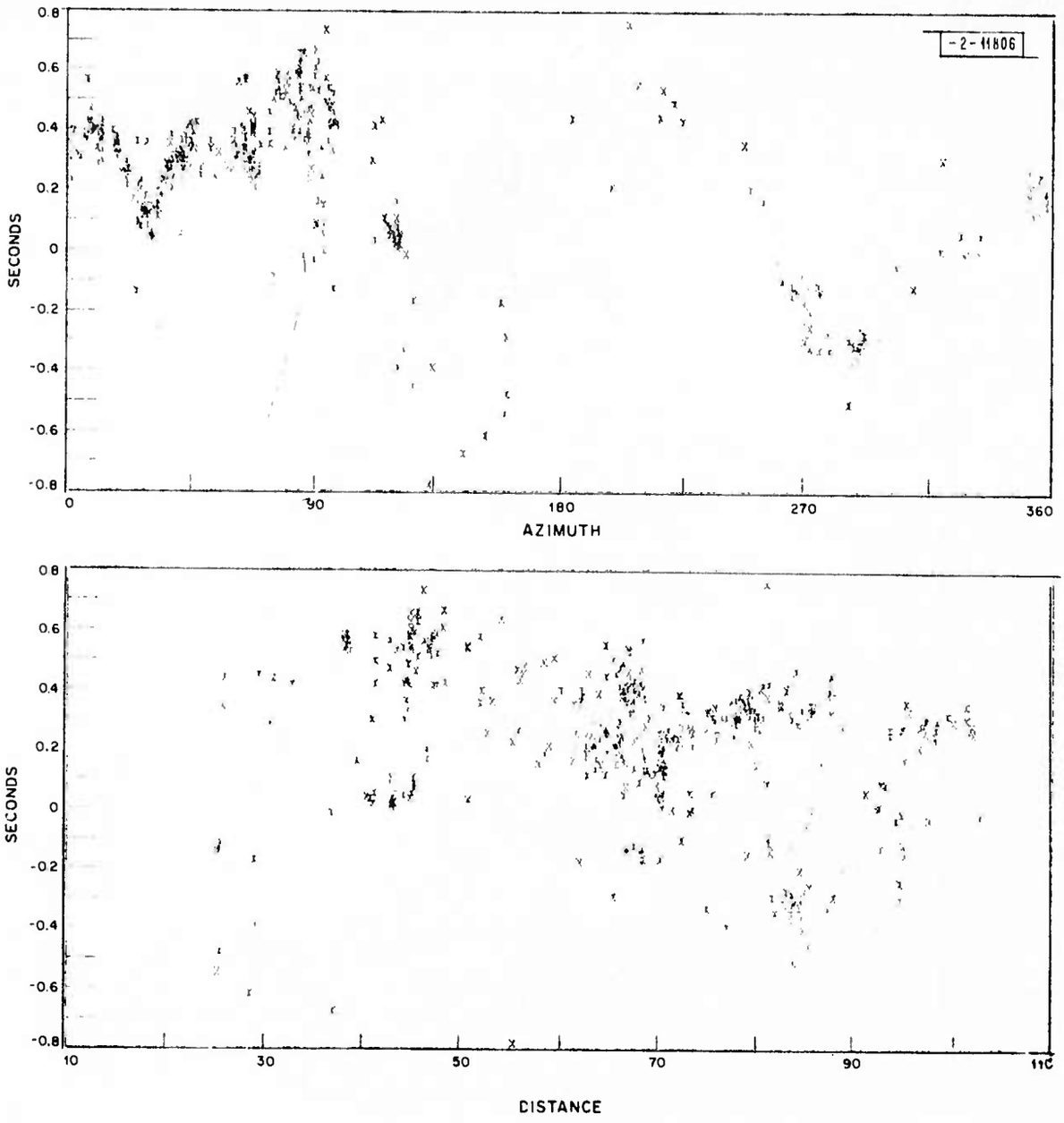

Fig. VII-2. Actual time delay errors for NORSAR subarray 03C.

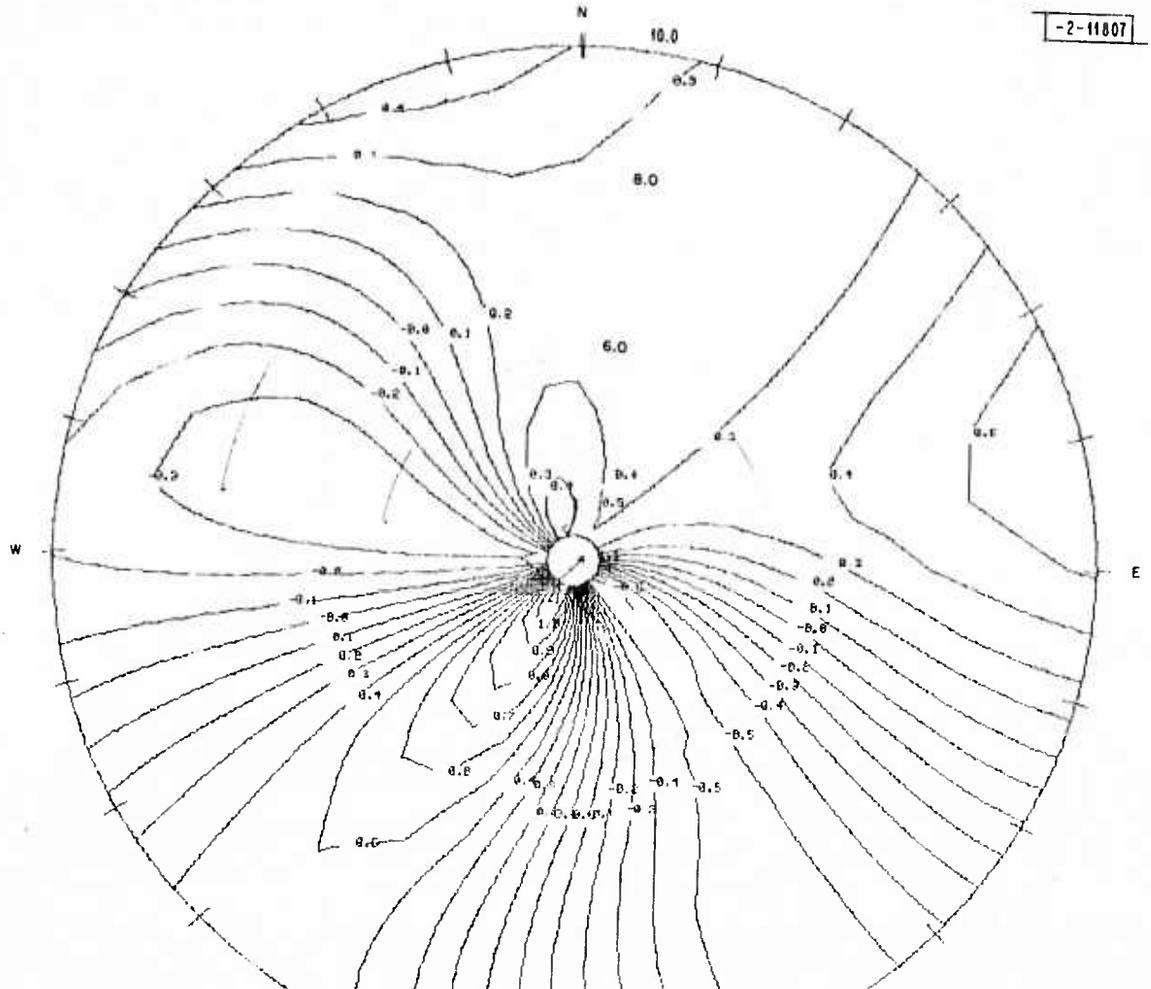

Fig. VII-3. Final station time correction for NORSAR subarray 03C. (Contours at 0.1 sec, radial component is $dT/d\Delta$.)

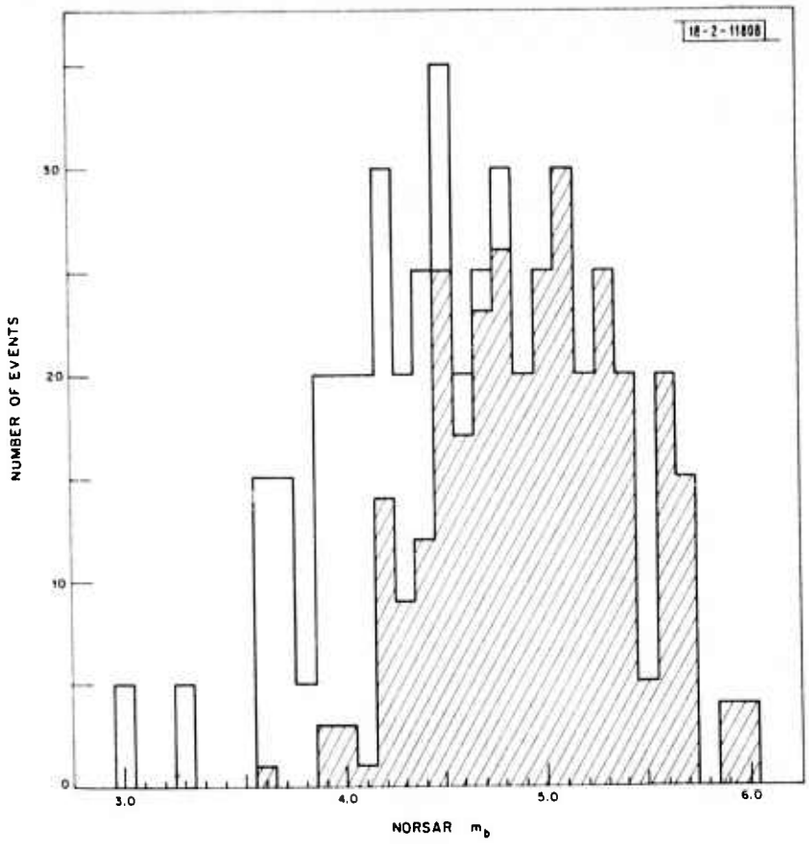

Fig. VII-4. Histogram of events as a function of NORSAR m_b. Shaded area indicates detected events, and unshaded area shows undetected events.

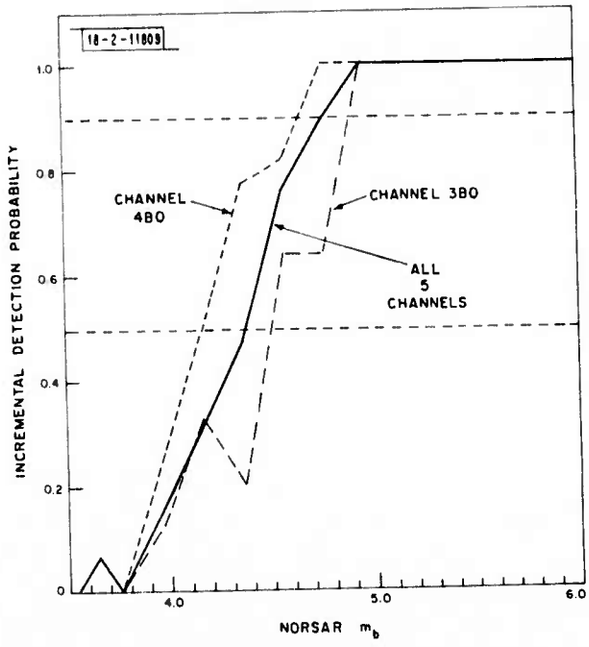

Fig. VII-5. Incremental detection probability for detection scheme. Data of Fig. VII-4 were averaged over bins 0.2 magnitude wide. Solid curve equals ratio of detections to total events using averaged data. Also shown are detection probabilities for channels 3B0 and 4B0.

VIII. PUBLICATIONS LIST

The following list contains all publications by Lincoln Laboratory in fields related to Seismic Discrimination from 1963 to the present. Additions to this list will be included in future SATS.

Many of the older publications are no longer available. Requests for more recent reports or reprints should be addressed to:

The secretary,
Lincoln Laboratory Group 22
42 Carleton Street
Cambridge, MA 02142

1. J. G. Proakis and P. R. Drouilhet, "Performance of Coherent Detection Systems Using Decision Directed Channel Measurement," Group Report 64G-1, Lincoln Laboratory, M.I.T. (27 June 1963), DDC AD-409819.

2. J. G. Proakis, "Optimum Pulse Transmissions for Multipath Channels," Group Report 64G-3, Lincoln Laboratory, M.I.T. (16 August 1963), DDC AD-416639.

3. P. L. Fleck, Jr. and T. J. Goblick, Jr., "Computer Programs for Processing Signals Received in Radar Astronomy Experiments," Group Report 64G-4, Lincoln Laboratory, M.I.T. (16 August 1963), DDC AD-419091.

4. R. Price, "The Doubly Non-Central F-Distribution Expressed in Finite Terms," Group Report 64G-5, Lincoln Laboratory, M.I.T. (13 September 1963), DDC AD-420434.

5. N. M. Abramson, "Further Considerations in the Use of Large Seismometer Arrays," Group Report 64G-6, Lincoln Laboratory, M.I.T. (14 November 1963), DDC AD-424594.

6. E. J. Kelly and M. J. Levin, "Signal Parameter Estimation for Seismometer Arrays," Technical Report 339, Lincoln Laboratory, M.I.T. (8 January 1964), DDC AD-435489.

7. E. J. Kelly, "The Representation of Seismic Waves in Frequency-Wave Number Space," Technical Note 1964-15, Lincoln Laboratory, M.I.T. (4 March 1964), DDC AD-433611.

8. Seismic Discrimination Semiannual Technical Summary, Lincoln Laboratory, M.I.T. (30 June 1964), DDC AD-443444.

9. E. J. Kelly, Jr., "Limited Network Processing of Seismic Signals," Technical Note 1964-44, Lincoln Laboratory, M.I.T. (4 September 1964), DDC AD-447220.

10. J. S. Richters, "The Application of Analysis of Variance to the Seismic Discrimination Problem," Technical Note 1964-60, Lincoln Laboratory, M.I.T. (3 November 1964), DDC AD-451871.

11. E. J. Kelly, Jr., "Random Scatter Channels," Technical Note 1964-61, Lincoln Laboratory, M.I.T. (4 November 1964), DDC AD-451756.

12. M. J. Levin, "Bounds on the Inverse of a Positive Definite Symmetric Matrix," Technical Note 1964-67, Lincoln Laboratory, M.I.T. (20 November 1964), DDC AD-452772.

13. Seismic Discrimination Semiannual Technical Summary, Lincoln Laboratory, M.I.T. (31 December 1964), DDC AD-455743.

14. P. E. Green, Jr., "A Large Aperture Seismic Array," Technical Note 1965-1, Lincoln Laboratory, M.I.T. (6 January 1965), DDC AD-609851.

15. M. J. Levin, "A Method for Power Spectrum Parameter Estimation," Technical Note 1965-8, Lincoln Laboratory, M.I.T. (10 February 1965), DDC AD-612796.

16. E. J. Kelly, Jr., "A Comparison of Seismic Array Processing Schemes," Technical Note 1965-21, Lincoln Laboratory, M.I.T. (14 June 1965), DDC AD-618017.

17. R. Price, "Statistical Synthesis of a pP-Wave Enhancer," Technical Note 1965-22, Lincoln Laboratory, M.I.T. (14 June 1965), DDC AD-617951.

18. R. Price, "An Approach to Estimation in Seismic Equalization," Technical Note 1965-24, Lincoln Laboratory, M.I.T. (28 June 1965), DDC AD-619020.

19. Seismic Discrimination Semiannual Technical Summary, Lincoln Laboratory, M.I.T. (30 June 1965), DDC AD-467395.

20. E. Gehrels, "A Review of Long-Range Earth Strain Measurement Techniques for Providing Earthquake Warning," Technical Note 1965-62, Lincoln Laboratory, M.I.T. (13 December 1965), DDC AD-625817.

21. J. Capon and R. J. Greenfield, "Asymptotically Optimum Multidimensional Filtering for Sampled-Data Processing of Seismic Arrays," Technical Note 1965-57, Lincoln Laboratory, M.I.T. (17 December 1965), DDC AD-626180.

22. M. Adler, "Noise and Low-Frequency Amplifiers," Technical Note 1965-52, Lincoln Laboratory, M.I.T. (21 December 1965), DDC AD-476983.

23. R. T. Lacoss, "Geometry and Patterns of Large Aperture Seismic Arrays," Technical Note 1965-64, Lincoln Laboratory, M.I.T. (31 December 1965), DDC AD-628148.

24. Seismic Discrimination Semiannual Technical Summary, Lincoln Laboratory, M.I.T. (31 December 1965), DDC AD-630559.

25. R. V. Wood, Jr., R. G. Enticknap, C. S. Lin and R. M. Martinson," Large Aperture Seismic Array Signal Handling System," Proc. IEEE 53, 1844-1851 (1965), DDC AD-632146.

26. H. W. Briscoe and P. L. Fleck, "Data Recording and Processing for the Experimental Large Aperture Seismic Array," Proc. IEEE 53, 1852-1859 (1965), DDC AD-632147.

27. P. E. Green, Jr., R. A. Frosch and C. F. Romney, "Principles of an Experimental Large Aperture Seismic Array (LASA)," Proc. IEEE 53, 1821-1833 (1965), DDC AD-632150.

28. J. F. Claerbout, "A Summary, by Illustrations, of Least Squares Filters with Constraints," Technical Note 1966-7, Lincoln Laboratory, M.I.T. (31 January 1966), DDC AD-629968.

29. H. W. Briscoe, J. Capon, P. L. Fleck, Jr., P. E. Green, Jr., R. J. Greenfield and E. J. Kelly, Jr., "Interim Report on Capabilities of the Experimental Large Aperture Seismic Array," Technical Note 1966-16, Lincoln Laboratory, M.I.T. (24 February 1966), DDC AD-631285.

30. J. Capon, R. J. Greenfield and R. J. Kolker, "A Frequency-Domain Synthesis Procedure for Multidimensional Maximum-Likelihood Processing of Seismic Arrays," Technical Note 1966-29, Lincoln Laboratory, M.I.T. (6 May 1966), DDC AD-634233.

31. Seismic Discrimination Semiannual Technical Summary, Lincoln Laboratory, M.I.T. (30 June 1966), DDC AD-637308.

32. E. J. Kelly, "LASA – On-Line Detection, Location and Signal-to-Noise Enhancement," Technical Note 1966-36, Lincoln Laboratory, M.I.T. (1 July 1966), DDC AD-636144.

33. J. Capon, R. J. Greenfield and R. T. Lacoss, "Off-Line Signal Processing Results for the Large Aperture Seismic Array," Technical Note 1966-37, Lincoln Laboratory, M.I.T. (11 July 1966), DDC AD-637016.

34. H. W. Briscoe and R. M. Sheppard, "A Study of the Capability of a LASA to Aid the Identification of a Seismic Source," Technical Note 1966-38, Lincoln Laboratory, M.I.T. (11 July 1966), DDC AD-437440.

35. P. E. Green, Jr. and R. V. Wood, Jr., "Large Aperture Seismic Array Capabilities," Technical Report 421, Lincoln Laboratory, M.I.T. (12 July 1966), DDC AD-631559.

36. E. Gehrels and L. G. Kraft, "A Computer Signal-Processing Approach for the Shapiro Fourth Test of the General Theory of Relativity," Technical Note 1966-23, Lincoln Laboratory, M.I.T. (2 September 1966), DDC AD-639733.

37. P. E. Green, Jr., "Seismic Data Collection," Proc. IBM Scientific Computing Symp. on Environmental Sciences, Yorktown Heights, November 1966, DDC AD-661154.

38. Seismic Discrimination Semiannual Technical Summary, Lincoln Laboratory, M.I.T. (31 December 1966), DDC AD-646677.

39. P. E. Green, Jr., E. J. Kelly, Jr. and M. J. Levin, "A Comparison of Seismic Array Processing Methods," Geophys. J. R. Astr. Soc. 11, 67-84 (1966), DDC AD-649184.

40. P. L. Fleck, "FASTABUL (A Fast Automatic STAtion BULletin Program)," Technical Notc 1967-3, Lincoln Laboratory, M.I.T. (6 January 1967), DDC AD-646207.

41. J. Capon, R. J. Greenfield and R. T. Lacoss, "Design of Seismic Arrays for Efficient On-Line Beamforming," Technical Note 1967-26, Lincoln Laboratory, M.I.T. (27 June 1967), DDC AD-655142.

42. E. J. Kelly, "Response of Seismic Arrays to Wide-Band Signals," Technical Note 1967-30, Lincoln Laboratory, M.I.T. (29 June 1967), DDC AD-656344.

43. Seismic Discrimination Semiannual Technical Summary, Lincoln Laboratory, M.I.T. (30 June 1967), DDC AD-657327.

44. R. M. Sheppard, Jr., "Values of LASA Time Station Residuals, Velocity and Azimuth Errors," Technical Note 1967-44, Lincoln Laboratory, M.I.T. (8 September 1967), DDC AD-662004.

45. J. Capon, R. J. Greenfield and R. T. Lacoss, "Long-Period Signal Processing Results for Large Aperture Seismic Array," Technical Note 1967-50, Lincoln Laboratory, M.I.T. (15 November 1967), DDC AD-663429.

46. P. E. Green and R. J. Greenfield, "Application of Large Aperture Array Techniques to Tsunami Warning," Technical Note 1967-58, Lincoln Laboratory, M.I.T. (29 December 1967), DDC AD-828319.

47. Seismic Discrimination Semiannual Technical Summary, Lincoln Laboratory, M.I.T. (31 December 1967), DDC AD-664872.

48. J. Capon, R. J. Greenfield and R. J. Kolker, "Multidimensional Maximum-Likelihood Processing of a Large Aperture Seismic Array," Proc. IEEE 55, 192-211 (1967), DDC AD-651722.

49. P. E. Green, Jr., "Recent Experiments with a Large Aperture Seismic Array," Proc. Intl. Union of Geodesy and Geophysics General Assembly, Special ASPEI Session on Arrays, Zurich, October 1967, DDC AD-688281.

50. R. M. Sheppard, E. J. Kelly and H. W. Briscoe, "Some Observations of Weak Japanese Earthquakes at the Montana LASA," Technical Note 1968-3, Lincoln Laboratory, M.I.T. (8 January 1968), DDC AD-665122.

51. R. T. Lacoss, J. Capon and R. J. Greenfield, "Preliminary Design of a Long-Period Seismic Array for Norway," Technical Note 1968-4, Lincoln Laboratory, M.I.T. (24 January 1968), DDC AD-665424.

52. E. J. Kelly, "A Study of Two Short-Period Discriminants," Technical Note 1968-8, Lincoln Laboratory, M.I.T. (12 February 1968), DDC AD-666701.

53. J. Capon, "Investigation of Long Period Noise at LASA," Technical Note 1968-15, Lincoln Laboratory, M.I.T. (3 June 1968), DDC AD-671509.

54. P. L. Fleck, "A Seismic Data Analysis Console," Technical Note 1968-14, Lincoln Laboratory, M.I.T. (19 June 1968), DDC AD-671961.

55. Seismic Discrimination Semiannual Technical Summary, Lincoln Laboratory, M.I.T. (30 June 1968), DDC AD-673354.

56. R. M. Sheppard, Jr., "Determination of LASA Detection and Location Ability Using Kurile Islands Events," Technical Note 1968-23, Lincoln Laboratory, M.I.T. (1 October 1968), DDC AD-678515.

57. Seismic Discrimination Semiannual Technical Summary, Lincoln Laboratory, M.I.T. (31 December 1968), DDC AD-682297.

58. J. Capon and P. E. Green, Jr., "Recent Results from the Large-Aperture Seismic Array," Nuovo Cimento Suppl. Ser. 1, 6, 82-95 (1968), DDC AD-688026.

59. J. Capon, R. J. Greenfield, R. J. Kolker and R. T. Lacoss, "Short-Period Signal Processing Results for the Large Aperture Seismic Array," Geophysics 33, 452-472 (1968), DDC AD-674830.

60. R. T. Lacoss, "Adaptive Combining of Wideband Array Data for Optimal Reception," IEEE Trans. Geosci. Electron. GE-6, 78-86 (1968), DDC AD-673599.

61. M. N. Toksöz and R. T. Lacoss, "Microseisms: Mode Structure and Sources," Science 159, 872 (1968), DDC AD-698577.

62. R. W. Ward, "Preliminary Long-Period Discrimination Results from NORSAR," Technical Note 1969-10, Lincoln Laboratory, M.I.T. (13 February 1969), DDC AD-686419.

63. R. T. Lacoss, "A Large-Population LASA Discrimination Experiment," Technical Note 1969-24, Lincoln Laboratory, M.I.T. (8 April 1969), DDC AD-687478.

64. E. Gehrels, "Interferometric Phase and Amplitude Fluctuation Measurements Over a 7-km Atmospheric Path," Technical Note 1969-28, Lincoln Laboratory, M.I.T. (13 May 1969), DDC AD-692438.

65. Seismic Discrimination Semiannual Technical Summary, Lincoln Laboratory, M.I.T. (30 June 1969), DDC AD-691434.

66. R. T. Lacoss, "LASA Decision Probabilities for $M_S - m_b$ and Modified Spectral Ratio," Technical Note 1969-40, Lincoln Laboratory, M.I.T. (23 July 1969), DDC AD-692451.

67. E. J. Kelly and R. T. Lacoss, "Estimation of Seismicity and Network Detection Capability," Technical Note 1969-41, Lincoln Laboratory, M.I.T. (16 September 1969), DDC AD-695044.

68. Seismic Discrimination Semiannual Technical Summary, Lincoln Laboratory, M.I.T. (31 December 1969), DDC AD-700322.

69. J. Capon, R. J. Greenfield and R. T. Lacoss, "Long-Period Signal Processing Results for the Large Aperture Seismic Array," Geophysics 34, 305-329 (1969), DDC AD-694326.

70. R. J. Greenfield and R. M. Sheppard, "The Moho Depth Variations under the LASA and Their Effect on dT/dΔ Measurements," Bull. Seismol. Soc. Am. 59, 409-420 (1969).

71. R. T. Lacoss, E. J. Kelly and M. N. Toksöz, "Estimation of Seismic Noise Structure Using Arrays," Geophysics 34, 21-38 (1969), DDC AD-688564.

72. J. Capon, "Investigation of Long-Period Noise at the Large Aperture Seismic Array," J. Geophys. Res. 74, 3182-3194 (1969).

73. J. Capon, "High-Resolution Frequency-Wavenumber Spectrum Analysis," Proc. IEEE 57, 1408-1418 (1969), DDC AD-696880.

74. J. Capon, "Signal Processing Results for Continental Aperture Seismic Array," Technical Note 1970-15, Lincoln Laboratory, M.I.T. (15 May 1970), DDC AD-707863.

75. Seismic Discrimination Semiannual Technical Summary, Lincoln Laboratory, M.I.T. (30 June 1970), DDC AD-710613.

76. J. R. Filson, "On Estimating Explosive Source Parameters at Teleseismic Distances," Technical Note 1970-9, Lincoln Laboratory, M.I.T. (8 July 1970), DDC AD-709767.

77. R. T. Lacoss and G. T. Kuster, "Processing a Partially Coherent Large Seismic Array for Discrimination," Technical Note 1970-30, Lincoln Laboratory, M.I.T. (27 November 1970), DDC AD-715917.

78. B. R. Julian, "Ray Tracing in Arbitrarily Heterogeneous Media," Technical Note 1970-45, Lincoln Laboratory, M.I.T. (31 December 1970), DDC AD-720795.

79. Seismic Discrimination Semiannual Technical Summary, Lincoln Laboratory, M.I.T. (31 December 1970), DDC AD-718971.

80. C. W. Frasier, "Discrete Time Solution of Plane P-SV Waves in a Plane Layered Medium," Geophysics 35, 197-219 (1970).

81. J. Capon and P. E. Green, "Statistical Accuracy of Data Used in Seismic Inversion," Geophys. J. 21, 373-386 (1970), DDC AD-723744.

82. J. Filson, "S Velocities at Near Distances in Western Central California," Bull. Seismol. Soc. Am. 60, 901-915 (1970), DDC AD-710446.

83. J. Capon, "Applications of Detection and Estimation Theory to Large Array Seismology," Proc. IEEE 58, 760-770 (1970), DDC AD-714323.

84. J. R. Filson, "Long Period SH_n," Bull. Seismol. Soc. Am. 60, 1297-1307 (1970), DDC AD-714317.

85. R. T. Lacoss, "Comments on 'A Simple Adaptive Algorithm for Real-Time Processing in Antenna Arrays'," Proc. IEEE (Letters) 58, 797-798 (1970).

86. J. Capon, "Analysis of Rayleigh-Wave Multipath Propagation at LASA," Bull. Seismol. Soc. Am. 60, 1701-1731 (1970), DDC AD-716084.

87. J. Capon and N. R. Goodman, "Probability Distributions for Estimators of the Frequency-Wavenumber Spectrum," Proc. IEEE 58, 1785-1786 (1970), DDC AD-723788.

88. D. P. McKenzie, D. Davies and P. Molnar, "Plate Tectonics of the Red Sea and East Africa," Nature 226, 243 (1970).

89. C. W. Frasier, "Seismic Scaling of Explosive Source Functions Using Teleseismic P Waves," Technical Note 1971-11, Lincoln Laboratory, M.I.T. (14 April 1971), DDC AD-723638.

90. J. F. Evernden and J. Filson, "Regional Dependence of Surface-Wave versus Body-Wave Magnitudes," J. Geophys. Res. 76, 3303-3308 (1971).

91. Seismic Discrimination Semiannual Technical Summary, Lincoln Laboratory, M.I.T. (30 June 1971), DDC AD-728210.

92. M. Mohajeri, "Statistics of the Spectral Ratio and Log-Likelihood Ratio Seismic Discriminants," Technical Note 1971-33, Lincoln Laboratory, M.I.T. (24 September 1971), DDC AD-731158.

93. R. T. Lacoss, "Seismic Event Detection and Discrimination – Some Statistical Considerations," in Proceedings from the Seminar on Seismology and Seismic Arrays, Oslo, 22-25 November 1971.

94. Seismic Discrimination Semiannual Technical Summary, Lincoln Laboratory, M.I.T. (31 December 1971), DDC AD-737092.

95. J. Capon, "Improvement in Seismic Discrimination Capability Using LASA," NEREM 13, Pt. 1, 245-247 (1971), DDC AD-738711.

96. R. T. Lacoss, "Data Adaptive Spectral Analysis Methods," Geophysics 36, 661-675 (1971), DDC AD-734104.

97. J. Capon and J. F. Evernden, "Detection of Interfering Rayleigh Waves at LASA," Bull. Seismol. Soc. Am. 61, 807-849 (1971), DDC AD-734105.

98. J. Capon, "Comparison of Love- and Rayleigh-Wave Multipath Propagation at LASA," Bull. Seismol. Soc. Am. 61, 1327-1344 (1971), DDC AD-736302.

99. M. N. Toksöz, J. W. Minear and B. R. Julian, "Temperature Field and Geophysical Effects of a Downgoing Slab," J. Geophys. Res. 76, 1113-1138 (1971).

100. D. Davies, E. J. Kelly and J. R. Filson, "Vespa Process for the Analysis of Seismic Signals," Nature 232, 8-13 (1971), DDC AD-737951.

101. P. L. Fleck and L. J. Turek, "A Seismic Data Analysis Console," Technical Report 495, Lincoln Laboratory, M.I.T. (18 January 1972), DDC AD-740604.

102. Seismic Discrimination Semiannual Technical Summary, Lincoln Laboratory, M.I.T. (30 June 1972), DDC AD-748305.

103. J. Filson and C. W. Frasier, "Multisite Estimation of Explosive Source Parameters," J. Geophys. Res. 77, 2045-2061 (1972), DDC AD-744889.

104. C. W. Frasier and J. Filson, "A Direct Measurement of the Earth's Short-Period Attenuation Along a Teleseismic Ray Path," J. Geophys. Res. 77, 3782-3787 (1972).

105. B. R. Julian, D. Davies and R. M. Sheppard, "PKJKP," Nature 235, 317-318 (1972), DDC AD-744396.

106. D. Davies, "Nocturnal Earthquakes," Geophys, J. R. Astr. Soc. 28, 305 (1972), DDC AD-752987.

107. D. Davies and B. R. Julian, "A Study of Short Period P-Wave Signals from Longshot," Geophys. J. R. Astr. Soc. 29, 185-202 (1972).

108. C. W. Frasier, "Observations of pP in the Short Period Phases of NTS Explosions Recorded at Norway," Geophys. J. R. Astr. Soc. 31, 99-109 (1972).

109. J. R. Filson and H. Bungum, "Initial Discrimination Results from the Norwegian Seismic Array," Geophys. J. R. Astr. Soc. 31, 315-328 (1972), DDC AD-763578.

110. T. E. Landers, "Some Interesting Central Asian Events on the M_S:m_b Diagram," Geophys. J. R. Astr. Soc. 31, 329-339 (1972).

111. J. Capon, "Long-Period Signal Processing Results for LASA, NORSAR, and ALPA," Geophys. J. R. Astr. Soc. 31, 279-296 (1972), DDC AD-771882.

112. D. Davies and A. M. Ziolkowski, "Observations of Short-Period Seismic Energy from Earthquakes and Inferences about the Seismic Source," Geophys. J. R. Astr. Soc. 31, 131-139 (1972), DDC AD-763575.

113. D. Davies and R. M. Sheppard, "Lateral Heterogeneity in the Earth's Mantle," Nature 239, 318-323 (1972), DDC AD-758942.

114. Seismic Discrimination Semiannual Technical Summary, Lincoln Laboratory, M.I.T. (31 December 1972), DDC AD-757560.

115. Seismic Discrimination Semiannual Technical Summary, Lincoln Laboratory, M.I.T. (30 June 1973), DDC AD-766559/9.

116. D. Davies and R. T. Lacoss, "First Results from the International Seismic Month," Technical Note 1973-32, Lincoln Laboratory, M.I.T. (2 July 1973), DDC AD-762921.

117. J. R. Filson, "On Estimating the Effect of Asian Earthquake Codas on the Explosion Detection Capability of LASA," Technical Note 1973-29, Lincoln Laboratory, M.I.T. (13 July 1973), DDC AD-767878.

118. Seismic Discrimination Semiannual Technical Summary, Lincoln Laboratory, M.I.T. (31 December 1973), DDC AD-777151.

119. J. Filson, T. Simkin and L. Leu, "Seismicity of a Caldera Collapse: Galapagos Islands 1968," J. Geophys. Res. 78, 8591-8622 (1973), DDC AD-777554.

120. D. Davies, "Monitoring Underground Explosions," Nature 241, 19-24 (1973), DDC AD-772138/4.

121. D. Davies, "Seismology with Large Arrays," in Reports on Progress in Physics, Vol. 36 (The Institute of Physics, London, 1973), pp. 1233-1283, DDC AD-771893/5.

122. A. Ziolkowski, "Prediction and Suppression of Long Period Nonpropagating Seismic Noise," Bull. Seismol. Soc. Am. 63, 937-958 (1973), DDC AD-772222/6.

123. D. K. Chowdhury and C. W. Frasier, "Observations of PcP and P Phases at LASA at Distances from 26° to 40°," J. Geophys. Res. 78, 6021-6027 (1973), DDC AD-772139/2.

124. B. R. Julian and M. K. Sengupta, "Seismic Travel Time Evidence for Lateral Inhomogencity in the Deep Mantle," Nature 242, 443-447 (1973), DDC AD-777615.

125. J. Capon, "Analysis of Microseismic Noise at LASA, NORSAR, and ALPA," Geophys. J. R. Astr. Soc. 35, 39-54 (1973).

126. R. E. Needham and D. Davies, "Lateral Heterogeneity in the Deep Mantle from Seismic Body Wave Amplitudes," Nature 244, 152-153 (1973), DDC AD-774002/0.

127. R. T. Lacoss, R. E. Needham and B. R. Julian, "International Seismic Month Event List," Technical Note 1974-14, Lincoln Laboratory, M.I.T. (27 February 1974), DDC AD-776021/8.

128. J. R. Filson, "Long Period Results from the International Seismic Month," Technical Note 1974-15, Lincoln Laboratory, M.I.T. (4 March 1974), DDC AD-776089/5.

129. Seismic Discrimination Semiannual Technical Summary, Lincoln Laboratory, M.I.T. (30 June 1974).

130. T. E. Landers, "Elastic Scattering of Plane P-Waves at Irregular Boundaries in the Lower Crust," Earthquake Notes 45, 12-23 (1974).

131. J. Capon, "Characterization of Crust and Upper Mantle Structure under LASA as a Random Medium," Bull. Seismol. Soc. Am. 64, 235-266 (1974).